SPLASHLESS SHIP BOWS AND WAVELESS STERNS

by

M.A.D.MADURASINGHE

B.Sc(Physics),B.Sc.Hon(Maths),
M.Sc(Computer Sc)A.I.T.

Thesis submitted for the degree of Doctor of Philosophy
in the University of Adelaide,
Department of Applied Mathematics

Dec. 1986.

SUMMARY

In two-dimensional bow-like flows past a semi-infinite body, one must in general expect a free-surface discontinuity, in the form of a splash or spray jet. However, there is numerical evidence that special body shapes do exist for which this splash is absent.

In the first part of this thesis an attempt is made to demonstrate steady state flow for an arbitrary (non-special) bow shape. Such flows necessarily include a splash jet, i.e. a portion of the incident stream is deflected upward and backward in the form of a jet, which then (in the presence of gravity) falls freely forever. This problem is exactly solved here via hodograph techniques, but only for infinite Froude number, i.e. by letting $g = 0$.

In the middle part of the thesis, conditions are established on the bow geometry in order that it should be splash-free at zero gravity, by solving the mathematical problem exactly using complex variable techniques, assuming a continuous non-stagnant flow attachment at the extreme bow. Then solutions are obtained for finite non-zero gravity by solving a non-linear integral equation numerically. A class of splashless non-bulbous body geometries with a downward directed segment at the extreme of the bow, to which the free surface attaches tangentially, is discussed in detail.

In the final part of the thesis, the flows of interest possess a stagnation point at the attachment point and demand underwater bodies of bulbous type, in order to be splashless. The nature of the solutions is discussed, giving analytical evidence, and a numerical scheme is then presented. The variation in the bulb shape and

size with Froude number is discussed in detail. Figures and tables are given at the end of the each chapter.

Signed Statement

The contents of this thesis have not been submitted to any University for the purpose of obtaining any other degree or diploma. Also to the best of my knowledge and belief, the thesis contains no material previously published or written by another person, except where due reference is made in the text. The author consents to the thesis being made available for photocopying and loan if applicable if accepted for the award of the degree.

M.A.D.MADURASINGHE

ACKNOWLEDGEMENT

I wish to express my deepest gratitude to my supervisor Professor E.O.Tuck, for his invaluable guidance and critical suggestions throughout this study. His infectious enthusiasm, deep insight into the problem, and his experience on the subject has not only made work on this study a rewarding experience, but has given me pleasant memories which I shall continue to cherish for a long time.

I would like to especially thank Prof. R.Radok sincerely, for encouraging me to pursue further studies in Australia.

I am also thankful to Professors R.J.Hosking and S.B.P.Wickramasuriya for helping me in various ways throughout my career. Last, but by no means least I would like to thank my mother and wife for their continuous support.

The author acknowledges the scholarship offered by the University Research Grants Committee during the period spent on this research.

M.A.D.MADURASINGHE

TABLE OF CONTENTS

GENERAL INTRODUCTION

One of the most important problems in ship hydrodynamics concerns the wave resistance of the ship. In particular the resistance is strongly influenced by the flow pattern around the bow. The search for means to reduce or possibly to minimise this resistance has taken many directions. So far, one of the most significant solutions has been the development of a bulbous shape bow, that dates back to 700 or 800 B.C.

Due to the lack of adequate mathematical theories and related experimental results concerning the bulbous bow, as well as the added cost in their construction, until the nineteenth century many ships did not seem to have them and so were excluded from whatever advantages might have ensued.

The bulbous bow reappeared in the nineteenth century with the advent of mechanical propulsion. As a result of various developments in war-ship design, this bulbous bow became a distinctive feature at the beginning of the twentieth century. It was on hulls of this type that David W.Taylor[7](1911) did his experiments and observed a reduction of resistance and a hydrodynamic superiority in higher speed ranges. Taylor was convinced that a bulbous nose located deeply at the forefoot and of rounded shape would produce less wave drag, because of a newly created pressure pattern in the vicinity of the bow wave. Since then, bow wave phenomena have been studied experimentally and theoretically by many outstanding hydrodynamicists. From the modern hydrodynamicist's point of view, the wave resistance of the ship can be dissected into two parts: one associated

with the non-breaking waves that are radiated far away from the bow, and the other associated with the wave energy that is dissipated by breaking close to the bow. This situation was first described by Froude(1955).

The non-breaking part is the one which was of main concern to Taylor, and the classical work on use of bulbous bows to reduce non-breaking wave resistance is that of Inui [13,14,15,16,17]. The breaking resistance received little attention until Baba[8,9] showed its importance. Since then, many researchers have studied the bow wave-breaking both experimentally and theoretically. Dagan and et al [11], Inui et al [12] and Baba[10] demonstrated the effect of reducing wave-breaking resistance by a bulbous bow. The so-called breaking waves are not so simple that they can be described in a few words. The term bow-wave breaking was used by Baba[8] for the white waves which looked like a necklace of pearls surrounding the ship. This term implied a plunging type of breaking, as defined in Peregrine[8], which breaks down vortically at the bow, and which was related to a spray jet by Dagan and Tulin[11]. In the latter theoretical study of the phenomenon for two-dimensional steady flow, breaking of the free surface was assumed to be related to a local Taylor instability, and application of the stability criterion determined the value of the critical Froude number which characterized breaking. Dagan and Tulin's high Froude number solution was based on a model of a jet detaching from the bow and not returning to the flow field.

This free streamline discontinuity in the form of a spray jet was later discussed by Tuck and Vanden-Broeck[2] for the flow around semi-infinite bodies. They called flows without such jets "splashless" and pointed out that in general if the

flow direction is reversed, so solving a stern rather than bow flow problem, a train of waves can be expected at downstream infinity. On the other hand, if one has been able to construct a special stern flow without such waves, that flow can be reversed in direction to yield a splashless bow flow. Examples of such near-bow or near-stern flows were computed by Vanden-Broeck and Tuck[3] using series expansion in the Froude number, and also by Vanden-Broeck, Schwartz and Tuck[4]. These authors showed the existence of downstream waves for stern flows, but were not able to find continuous solutions without waves because of the restricted geometries they considered. However their work suggested that the wave-free and splash-free property may exist only for specially selected body geometries. Later, Vanden-Broeck and Tuck[5] studied linear and nonlinear free-surface flows under gravity in a two-dimensional framework, in which a disturbance was caused to an otherwise uniform stream by a distribution of pressure over the free surface. Even though such a disturbance, in general, creates a system of trailing waves, they observed the existence of special disturbances that do not have waves. Their work strongly suggested the existence of special splashless bow geometries. The investigation made by Schmidt[1] using linearized theory has also suggested such bow flows.

The flows of interest can possess a stagnation point at the attachment point, or alternatively can involve tangential (continuous) attachment. Tuck and Vanden-Broeck[2] demonstrated numerically one such bow shape with a stagnation point, and further suggested that those bow flows in which the splash drag component can be eliminated are of a bulbous character. These authors, using a numerical scheme, observed that a train of waves is present at infinity, downstream of a stern

or upstream of a bow, and then they succeeded in a search for that particular body geometry which made the wave amplitude vanish.

Subsequent work by Tuck and the present author (1985)[6] is contained in chapter 2, which concentrates upon the tangential attachment case. The corresponding mathematical problem is exactly solved here for infinite Froude number by letting $g = 0$ and then, for finite Froude numbers, a special numerical scheme which always forces itself to converge to a waveless solution is presented. This is achieved by letting the scheme estimate one of the unknown parameters determining the bow geometry. The results obtained seem more suitable for a waveless stern rather than for a bow, since all the so-derived bodies (which are in general *not* bulbous) demand a downward slope at attachment.

Chapter 3 of the thesis concentrates on splashless and waveless bows which involve conventional-type bulbous bows with a stagnation point at attachment. It is proved that such a flow has a locally horizontal free surface at attachment, if the angle to the horizontal of the body at the stagnation point is greater than 60^0. A numerical scheme similar to the above mentioned is then employed to obtain only splashless solutions, by allowing the scheme to change the body geometry accordingly. Numerical evidence indicates that wave-free stern flows, or equivalently splash-free bow flows with a stagnation point at attachment, demand underwater bodies of unique bulbous shape for $F > 0.54$, where F is the Froude number based on the draught of the ship. For $0.50 < F < 0.54$, this unique shape is non-bulbous and essentially rectangular. For $0.45 < F < 0.50$ there seems to exist two or three distinct solutions and consequently two or three quite different

bulb sizes that allow splash-free flows, and for $F < 0.45$, many solutions exist. The existence of many solutions for small Froude numbers ($F < 0.45$) supports the conclusion that body geometry is arbitrary in this range, in which gravity is effectively infinity and no stern creates waves.

A large collection of results is included, generalising the single case presented by Tuck and Vanden-Broeck[2]. In particular, variation in the bulb shape and size with Froude number is discussed in detail.

CHAPTER 1

SOME EXACT SOLUTIONS FOR SPLASHES AT INFINITE FROUDE NUMBER

1.1 Introduction

This approach is to compute steady state flow for an arbitrary (non-special) bow shape. Such flows necessarily include a splash jet, i.e. a portion of the incident stream is deflected upward and backward in the form of a jet, which then (in the presence of gravity) falls freely forever in an approximately parabolic trajectory (see Fig. 1.2a). The jet and the incident stream are supposed to passs across each other without interference. Mathematically they lie on distinct "Riemann Sheets".

These problems are exactly solved here only for infinite Froude number, i.e. by letting $g = 0$. In the presence of gravity these problems become extremely difficult numerical problems. First we consider a simplified version of this phenomenon where the attention is given only to the jet, which travels upward along the bow and corresponds to a horizontal channel at upstream infinity(Fig.1.1). Secondly, we formulate the general problem which takes in to consideration the flow underneath the body as well(Fig.1.2a). In this formulation there will be a submerged stagnation point where the dividing streamline intersects the body. Dagan and Tulin[11] studied this problem using perturbation expansions.

1.2 Formulation of the simplified problem

Let us consider a part of the incident stream which rises up the bow and deflects upwards (see Fig 1.1). At upstream infinity, there is a uniform stream of unit magnitude, in the form of a horizontal channel of width h. ABD is a fixed boundary wall, where the slope is specified without loss of generality from A($\phi = -\infty$) to D($\phi = 0$) as follows:

$$\theta = \begin{cases} 0, & -\infty < \phi < -1; \\ \Theta(\phi), & -1 < \phi < 0. \end{cases} \tag{1.1}$$

where $\Theta(\phi)$ is the slope of the curved section of the wall. It is assumed that the flow is irrotational and the fluid is inviscid and incompressible. Continuous flow attachment is assumed at D ($\phi = 0$), where the wall ends. Here ϕ is the potential function and ψ is the stream function. Let $\psi = 0$ on the wall and on the free streamline DE. Let $\psi = -1$ on the upper free streamline, which is completely free from $\phi = -\infty$ to $\phi = +\infty$, as seen in Figure 1.1. The complex velocity $u - iv$ is an analytic function of the complex potential $f = \phi + i\psi$, where u, v are the velocity components in the x and y directions respectively(see Fig1.1). The function $\tau - i\theta$ is defined by

$$\frac{df}{dz} = u - iv = \exp(\tau - i\theta). \tag{1.2}$$

In the presence of gravity, Bernoulli's equation and the condition of constant pressure on the free surface yield

$$e^{\tau} = |\frac{df}{dz}| = 1, \tag{1.3}$$

for $\psi = 0, 0 \leq \phi \leq +\infty$ and for $\psi = -1, \ -\infty < \phi < +\infty$.

1.3 Solution and its properties

Consider the potential function $f(z)$ given by the integration of

$$u - iv = \frac{df}{dz} = \exp \frac{1}{\pi} \int_{-1}^{0} \log \left(\frac{\sqrt{e^{-\pi f} - 1} + \sqrt{e^{-\pi s} - 1}}{\sqrt{e^{-\pi f} - 1} - \sqrt{e^{-\pi s} - 1}} \right) \Theta'(s) ds. \qquad (1.4)$$

This can be derived using a formula developed later (Chapter 2) and by applying the appropriate conformal transformations. However, it can be checked directly, as follows. It can be shown that (1.4) defines the complex velocity $u - iv$ as an analytic function of the complex potential $f = \phi + i\psi$ and satisfies the required conditions as follows.

(a) On $\psi = -1$, we have $f = \phi - i$ for $-\infty < \phi < +\infty$ and hence $|\frac{df}{dz}| = 1$, since $-1 \leq s \leq 0$ in the integrand. Also, we have $u - iv \to 1$ as $\phi \to -\infty$.

(b) On $\psi = 0, \phi > 0$ we can show $|\frac{df}{dz}| = 1$ as above.

(c) On $\psi = 0, -1 \leq \phi < 0$ we can write $\frac{df}{dz} = u - iv = R(\phi) e^{-i\Theta(\phi)}$ for some real function $R(\phi)$.

(d) On $\psi = 0, \phi < -1$ it is clear that $\frac{df}{dz} = u - iv$ is real and $u - iv \to 1$ as $\phi \to -\infty$.

Hence (1.4) gives the correct complex potential for the problem. Furthermore, (1.4) holds for continuous as well as discontinuous slopes. For polygonal barriers $\Theta'(s)ds$ in (1.4) should be interpreted as $\Theta'(s)ds = d\Theta = \Theta(s^+) - \Theta(s^-)$, where $\phi = s$ is the corner of the polygon. From (1.4) we can extract the free-streamline slope as follows.

$$\theta(\phi) = \frac{1}{\pi} \int_{s=-1}^{s=0} \tan^{-1} \left(\frac{2\sqrt{(1 - e^{-\pi\phi})(e^{-\pi s} - 1)}}{2 - e^{-\pi\phi} - e^{-\pi s}} \right) d\Theta \quad \text{for} \quad \psi = 0 \ \phi > 0, \qquad (1.5)$$

and

$$\theta(\phi) = \frac{1}{\pi}\int_{s=-1}^{s=0} \tan^{-1}\left(\frac{2\sqrt{(1+e^{-\pi\phi})(e^{-\pi s}-1)}}{2-e^{-\pi s}+e^{-\pi\phi}}\right) d\Theta \quad \text{on } \psi = -1. \tag{1.6}$$

The ultimate direction of the jet, θ_∞ (say), is obtained by letting $\phi \to +\infty$ in either of the above expressions. Hence we have

$$\begin{aligned}\theta_\infty &= \frac{1}{\pi}\int_{s=-1}^{s=0} \tan^{-1}\frac{2\sqrt{e^{-\pi s}-1}}{2-e^{-\pi s}} d\Theta \\ &= \frac{2}{\pi}\int_{s=-1}^{s=0} \tan^{-1}\sqrt{e^{-\pi s}-1}\, d\Theta.\end{aligned} \tag{1.7}$$

Consider for example a polygonal wall, where the slope is defined by

$$\begin{aligned}\Theta(\phi) &= \beta_1 \quad -\alpha < \phi < 0, \\ &= \beta_2 \quad -1 < \phi < -\alpha.\end{aligned} \tag{1.8}$$

The direction of the jet θ_∞ is given by (1.7) as

$$\theta_\infty = \frac{2}{\pi}\left(\beta_2 \tan^{-1}\sqrt{e^{\pi}-1} + (\beta_1-\beta_2)\tan^{-1}\sqrt{e^{\pi\alpha}-1}\right). \tag{1.9}$$

If $\theta_\infty > \pi$ then the jet falls back on the incident stream. But in this $g = 0$ case, to demonstrate this situation we have to define a downward directed segment at the end of the barrier(just before the point of detachment). If $g > 0$, this happens whenever $\theta_\infty > \frac{\pi}{2}$, of course.

We may expect a horizontal drag force F on the wall given by

$$F = \rho h(1-\cos\theta_\infty), \tag{1.10}$$

where ρ is the fluid density. x, y cordinates must be obtained by integrating

$$\frac{\partial y}{\partial \phi} = e^{-\tau}\sin\theta, \tag{1.11}$$

and

$$\frac{\partial x}{\partial \phi} = e^{-\tau}\cos\theta. \tag{1.12}$$

1.4 General problem

Consider the same two dimensional steady flow, but now around a blunt body of semi-infinite length (Figure 1.2a). A portion of the incident stream with thickness h at upstream infinity is deflected upward in the form of the jet. Let $\psi = 0$ on the free streamline AJ, where ϕ varies from $-\infty$ to $+\infty$. Let $\psi = -t$ on J'DSA' and on PS, where S is a submerged stagnation point and the section J'D is a free streamline. The slope is prescribed on the body, i.e on DSA' as $\theta = \Theta(\phi)$, $\phi_0 < \phi < \infty$, where ϕ is the potential function.

A continuous flow attachment is assumed at D ($\phi = \phi_0$). x and y axes are located as in Figure 1.2a, where the x axis merges with the bottom of the ship at downstream infinity on $\psi = -t$. H is the draught of the body and a flow field of unit magnitude is assumed at both downstream and upstream infinities.

The analytic functions f and $\tau - i\theta$ are defined as above, and we map f on the auxiliary half plane ξ plane by the transformation

$$f = \xi - \frac{t}{\pi} \log \xi, \tag{1.13}$$

where $\xi = X + iY$, and t is the jet thckness in the f plane.

Now let us identify some of the important points on the auxiliary plane $\xi = X + iY$ (Fig. 1.2c). $X = 0, Y = 0^-$ corresponds to JJ' (jet end), $X = \frac{t}{\pi}, Y = 0^-$ is the submerged stagnation point. Let the detachment point D corresponds to $X = X_0, Y = 0^-(0 < X_0 < \frac{t}{\pi})$. The relationship between X and ϕ is given by

$$\phi(X) = X - \frac{t}{\pi} \log |X|. \tag{1.14}$$

The slope of the ship bow (DSA') $\Theta(\phi)$ $\phi_0 < \phi < \infty$ will be used in the X scale by referring to $\Theta(\phi(X))$, $X_0 < X < \infty$. It should be noticed that $\Theta(\phi(X))$ represents the direction of the flow as well, i.e. $\Theta(\phi(X)) > 0$ for $X_0 < X < \frac{t}{\pi}$, $\Theta(\phi(X)) < 0$ for $\frac{t}{\pi} < X < \infty$ and $\Theta(\phi(X)) \to 0$ as $X \to +\infty$.

1.5 Solution and its properties

Consider the potential function $f(z)$ given by the integration of

$$u - iv = \frac{df}{dz} = \exp \frac{-1}{\pi} \int_{s=\infty}^{s=X_0} \log \left(\frac{\sqrt{\xi - X_0} - \sqrt{s - X_0}}{\sqrt{\xi - X_0} + \sqrt{s - X_0}} \right) d\Theta, \qquad (1.15)$$

where this integration is performed in the auxiliary plane along its real axis. In case of continuous slope, we require $d\Theta = \frac{d\Theta}{d\phi} \frac{d\phi}{ds}$, where $\frac{d\phi}{ds}$ must be obtained by differentiating (1.14). For polygonal bodies we have $d\Theta = \Theta(\phi(X_j^-)) - \Theta(\phi(X_j^+))$ where $\phi = \phi(X_j)$ is a corner of the polygon. It should be noted that there is a compulsory corner, due to the change of flow direction above and below the submerged stagnation point S. This solution also can be derived using formula (2.10) in chapter 2 and by the use of appropriate conformal mappings. However, it can be shown that (1.15) satisfies all the boundary conditions, by referring to the ξ plane. i.e.

(a) $|\frac{df}{dz}| = 1$ for $Y = 0^-, X < X_0$. This includes both free streamlines AJ and J'D. Further we have $\frac{df}{dz} \to 1$ as $X \to -\infty$.

(b) $Y = 0^-$, $X_0 < X < \infty$ we have $\frac{df}{dz} = R(\phi(X))e^{-i\Theta(\phi(X))}$ for some real function $R(\phi(X))$, where $R(\phi(X)) \to 1$ as $X \to +\infty$.

The free streamline slopes are given by

$$\theta(\phi) = \frac{1}{\pi}\int_{\infty}^{X_0} \tan^{-1}\left(\frac{-2\sqrt{(X_0 - X)(s - X_0)}}{s + X - 2X_0}\right) d\Theta, \quad X < X_0. \tag{1.16}$$

This includes both free streamlines, namely AJ and J'D for $-\infty < X < 0$ and $0 < X < X_0$ respectively. The ultimate direction θ_∞ of the jet is given at $X = 0$, i.e.

$$\theta_\infty = \frac{2}{\pi}\int_{\infty}^{X_0} \tan^{-1}\sqrt{\frac{s}{X_0} - 1} d\Theta. \tag{1.17}$$

For example let us consider a simple bow geometry, which consists of a vertical front and a flat bottom, as seen in Figure 1.3. This problem with a single corner was discussed by Oertel[18], and he obtained θ_∞ by inverting the related semi-infinite Hilbert transforms. The slope function can be given by

$$\Theta(\phi(X)) = \begin{cases} \frac{\pi}{2}, & \text{if } X_0 < X < \frac{t}{\pi}; \\ -\frac{\pi}{2}, & \text{if } \frac{t}{\pi} < X < 2; \\ 0, & \text{if } X > 2. \end{cases} \tag{1.18}$$

The potential function is given by(using (1.15))

$$\frac{df}{dz} = \left(\frac{\sqrt{\xi - X_0} - \sqrt{2 - X_0}}{\sqrt{\xi - X_0} + \sqrt{2 - X_0}}\right)^{1/2} \left(\frac{\sqrt{\xi - X_0} - \sqrt{t/\pi - X_0}}{\sqrt{\xi - X_0} + \sqrt{t/\pi - X_0}}\right)^{-1} \tag{1.19}$$

substituting $\theta(\phi(X))$ in (1.17) we have

$$\theta_\infty = 2\tan^{-1}\sqrt{\frac{t}{\pi X_0} - 1} - \tan^{-1}\sqrt{\frac{2}{X_0} - 1} \tag{1.20}$$

1.6 Concluding remarks

In this chapter we have solved the problems related to splashes at zero gravity. But application of gravity to any of the above formulations is extremly difficult. One has to first attempt to solve the simplified version of this problem in Fig.1.1 by using a numerical procedure. However, these exact solutions may be useful to check the accuracy and validity of such a numerical scheme near zero gravity.

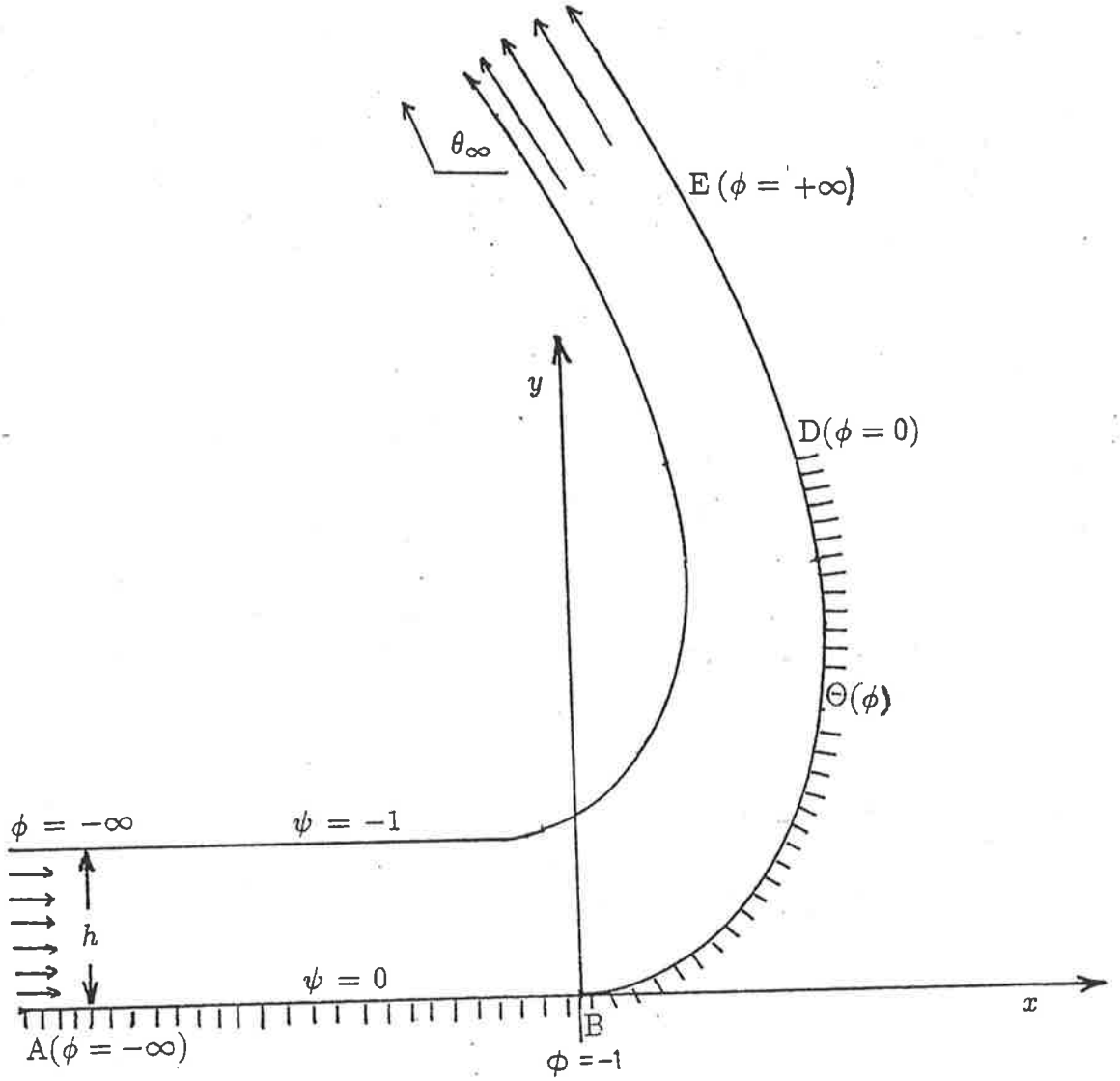

Figure 1.1: Uniform stream of unit magnitude meeting a fixed curved boubdary wall.

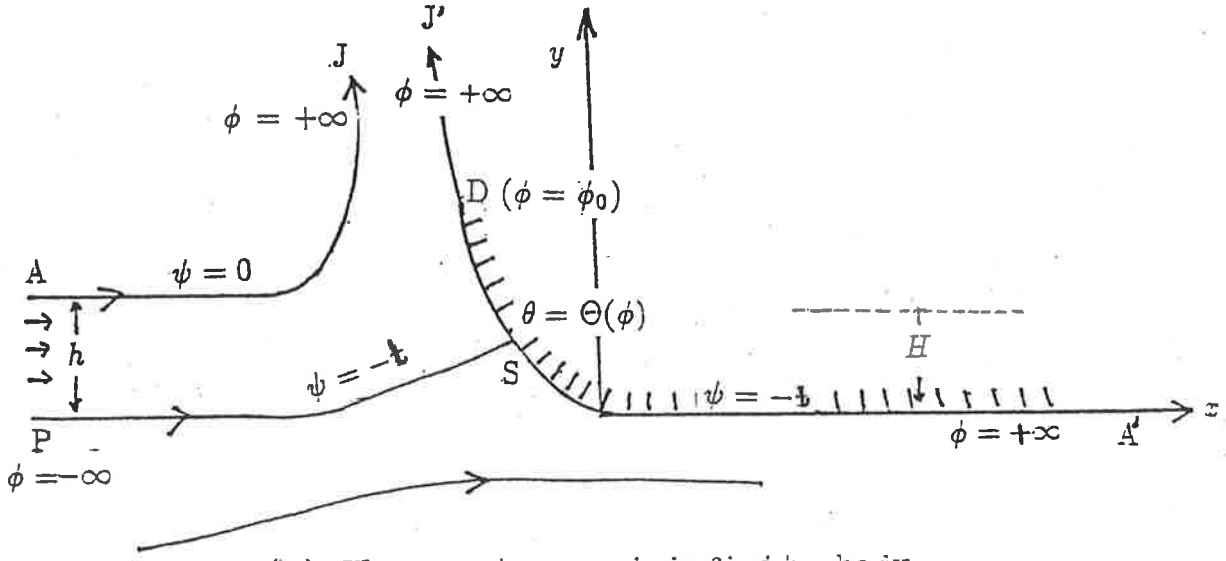

(a) Flow past a semi-infinite body .

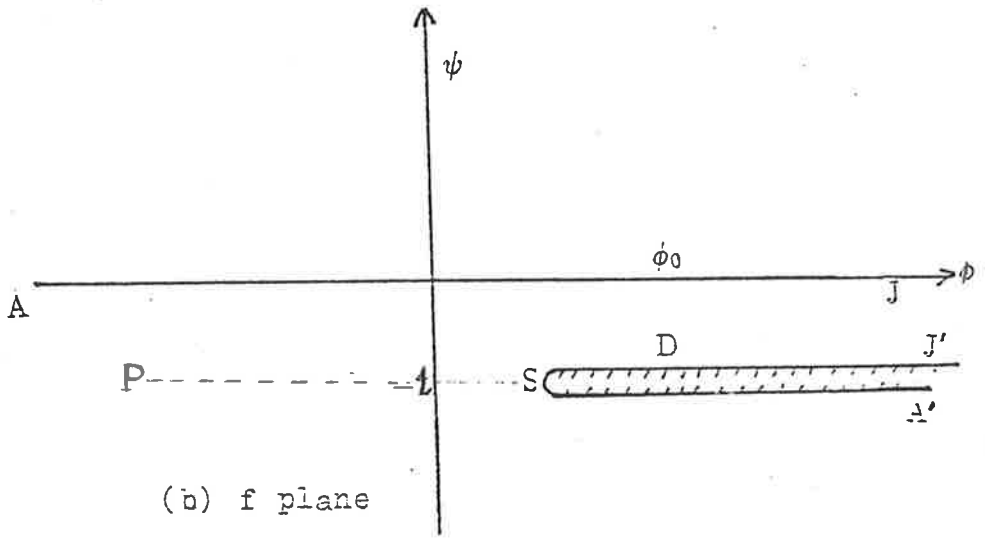

(b) f plane

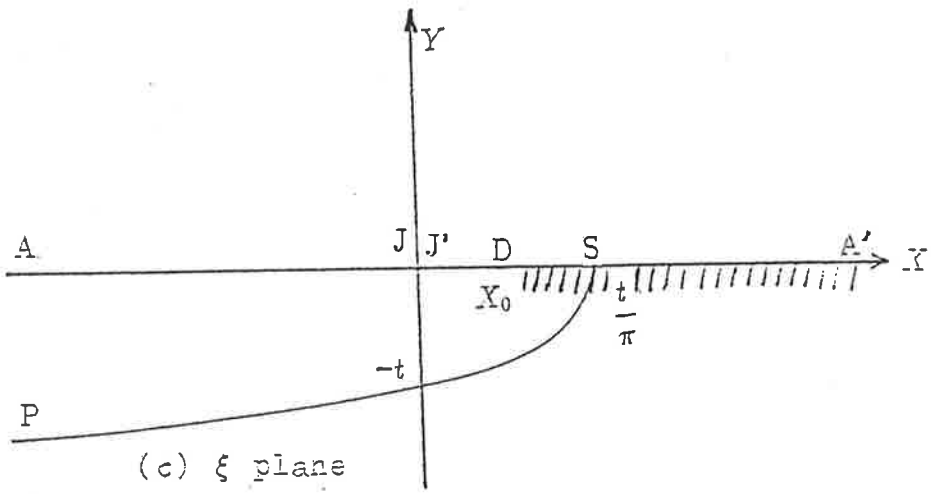

(c) ξ plane

Figure 1.2

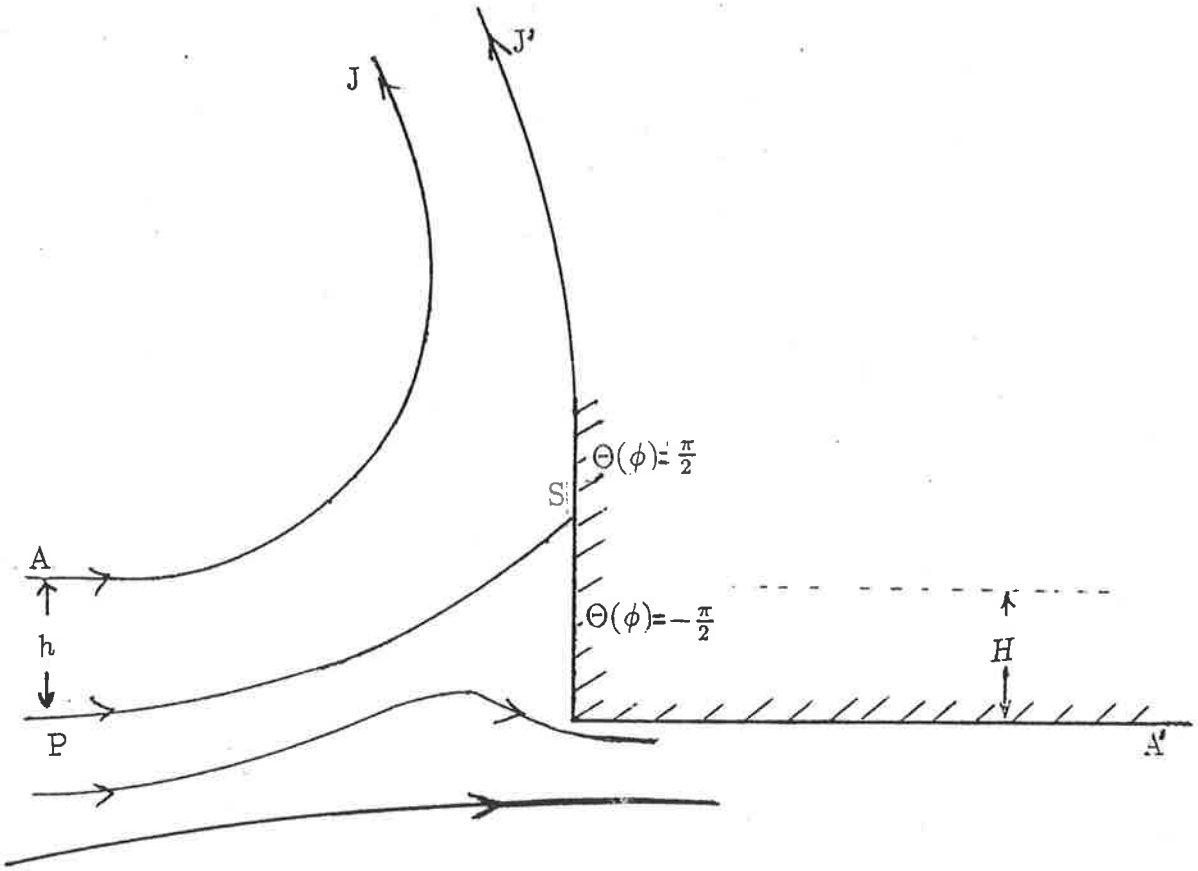

Figure 1.3: Potential flow past a simple bow geometry.

CHAPTER 2

SPLASHLESS SHIP BOWS OR WAVELESS STERNS WITH CONTINUOUS FLOW ATTACHMENT

2.1 Introduction

In this chapter we treat the free streamline problem associated with the flow at the bow of a ship within the framework of steady two-dimensional potential flow with the aim of deriving a bow geometry which possesses the desirable property of splashlessness or equivalently wavelessness. Our attention is strictly restricted here to the tangential attachment at the extreme bow where the flow separates.

First, conditions are established on the geometry of the bow, in order that it should be splash-free at zero gravity, i.e. for infinite Froude number. That is, we set $g = 0$, and solve the corresponding mathematical problem exactly by a hodograph method. This zero-gravity solution necessarily has either infinite or (exceptionally) zero draught, and those special solutions that have zero draught are selected for further attention. Numerical evidence then indicates that wave-free stern flows, or equivalently splash-free bow flows, exist for a finite range of gravity, i.e. for $0 \leq g < g_m$, where g_m is an upper bound which depends on the family of bow shapes considered. A numerical scheme which determines only such splashless solutions is employed to investigate the deformation of the original bow shape, as gravity increases from zero. This task is achieved by allowing the numerical scheme to adjust one of the parameters determining the geometry of the bow.

2.2 Formulation

Consider the steady two-dimensional irrotational flow of an inviscid incompressible infinitely-deep fluid past a semi-infinite body, whose bottom surface is the plane $y = -D$, for $x < 0$. A finite non-planar termination to the body lies in $x > 0$, and there is tangential free surface attachment at the point where the body ends. The flow underneath the body is assumed to approach a uniform stream of unit magnitude as $x \to -\infty$. The level $y = 0$ corresponds to the level of the free surface at which the velocity is equal to 1 when $x > 0$. In general, we expect a mean free-surface level $y = 0$ as $x \to +\infty$ and can interpret D as the "draught" of the body.

Let the potential function be ϕ, and the stream function be ψ. Choose $\phi = 0$ at the point of detachment of the free streamline and the body, and $\psi = 0$ on the free surface and on the surface of the body. Let the value of ϕ at $x = 0, y = -D$ be -1; thus the body is curved only in $-1 < \phi < 0$. Use of these dimensionless variables will be justified in the next chapter by referring them to a suitable velocity scale and a length scale. It should be noted that the draft-based Froude number is $1/\sqrt{gD}$. The complex velocity $u - iv$ is an analytic function of the complex potential $f = \phi + i\psi$, where u,v are the velocity components in the x and y directions respectively. The function $\tau - i\theta$ defined by

$$\frac{df}{dz} = u - iv = \exp(\tau - i\theta). \tag{2.1}$$

is an analytic function of f in the half plane $\psi \leq 0$, and tends to zero as $|f| \to \infty, \psi \leq 0$. Therefore, on $\psi = 0$, its real part is the Hilbert transform of its

imaginary part, and we have

$$\tau(\phi) = \frac{1}{\pi}\int_{-\infty}^{+\infty} \frac{\theta(\varphi)}{\varphi - \phi} d\varphi, \tag{2.2}$$

where $\tau(\phi)$ and $\theta(\phi)$ denote respectively $\tau(\phi, 0_-)$ and $\theta(\phi, 0_-)$. The integral in (2.2) is to be interpreted in the Cauchy principal-value sense. The kinematic condition on the body yields

$$\theta = 0, \qquad \psi = 0, \phi < -1, \tag{2.3}$$

$$\theta = \Theta(\phi), \quad \psi = 0, -1 < \phi < 0. \tag{2.4}$$

Here the function $\Theta(\phi)$ defines the shape of the body. An important special case is a polygonal body where $\Theta(\phi)$ is a step function, as sketched in Fig.2.1. Bernoulli's equation and the condition of constant pressure on the free surface yield

$$gy + \frac{1}{2}q^2 = \frac{1}{2}, \tag{2.5}$$

where y is given by

$$\frac{\partial y}{\partial \phi} = e^{-\tau} \sin\theta. \tag{2.6}$$

Differentiating (2.5) with respect to ϕ, using (2.6), and integrating gives

$$g\int_{\infty}^{\phi} \sin\theta d\varphi + \frac{1}{3}e^{3\tau} = \frac{1}{3}, \tag{2.7}$$

where the limits $y \to 0$ and $\tau \to 0$ as $\phi \to \infty$ have been enforced. Substituting (2.3), (2.4) and (2.7) into (2.2), we get

$$\int_0^{\infty} \frac{\theta(\varphi)}{\varphi - \phi} d\varphi + T(\phi) = \frac{\pi}{3}\log[1 - 3g\int_{\infty}^{\phi} \sin\theta d\varphi] \quad \text{for } \phi > 0, \tag{2.8}$$

where

$$T(\phi) = \int_{-1}^{0} \frac{\Theta(\varphi)}{\varphi - \phi} d\varphi. \tag{2.9}$$

$T(\phi)$ is a known function, for a given bow-shape function $\Theta(\phi)$.

For given $\Theta(\phi), -1 \leq \phi \leq 0$, the problem reduces to finding a function $\theta(\phi)$ satisfying the nonlinear integral equation (2.8) for $\phi > 0$. The exact solution to equation (2.8) in the absence of gravity is described in the next section. If $g > 0$, equation (2.8) must be solved numerically.

2.3 Zero gravity solution

In the previous chapter we solved exactly the problems related to splashes by setting $g = 0$. Those solutions (1.4) and (1.15) were obtained by mapping the flow fields on to a half plane and comparing the special solution we derive in this section for a well known problem in the history of hydrodynamics. In other words, the solution we may find for the problem in which the splash drag component is absent allows us to solve a variety of other problems including the one in which the splash is present.

As $g \to 0$, equation (2.7) indicates that $\tau \to 0$ on the free streamline; i.e. the fluid velocity is of constant (unit) magnitude. Potential flow past a curved obstacle with a constant-speed free boundary has been long recognized as an interesting mathematical problem, and questions of construction, calculation, existence, and uniqueness have intrigued many outstanding hydrodynamicists and mathematicians, see Gilbarg [20], Birkhoff & Zarantonello [19]. For simple configurations, such as flat plates, symmetric wedges, and other simple polygonal shapes with one

or two corners, the direct problem immediately admits a unique explicit solution by the hodograph method, see Wu [23], Milne-Thomson [22], Gilbarg [21].

Consider the potential function $f(z)$ given by integration of

$$u - iv = \frac{df}{dz} = \exp \int_{-1}^{0} \frac{\Theta'(s)}{\pi} \log \left(\frac{\sqrt{-f} + \sqrt{-s}}{\sqrt{-f} - \sqrt{-s}} \right) ds. \tag{2.10}$$

This could be derived as a limiting case of the Schwartz-Christoffel transformation in the hodograph plane, by adopting the following procedure which briefly explains the major steps only.

First we consider the simple geometry which has only one corner and hence, only one angled straight line segment as in figure 2.1 when $n = 0$. The potential function $f(z)$ is given by the integration of (see Milne-Thomson[22])

$$\frac{df}{dz} = u - iv = \left(\frac{\sqrt{-f} + 1}{\sqrt{-f} - 1} \right)^{\frac{\theta_0}{\pi}} \tag{2.11}$$

Using the same technique, we may now extend the above solution for a polygonal body with n corners (Fig.2.1) as

$$\frac{df}{dz} = \left(\frac{\sqrt{-f} + \sqrt{1}}{\sqrt{-f} - \sqrt{1}} \right)^{\bar{\theta}_n/\pi} \left(\frac{\sqrt{-f} + \sqrt{\alpha_{n-1}}}{\sqrt{-f} - \sqrt{\alpha_{n-1}}} \right)^{\frac{\bar{\theta}_{n-1} - \bar{\theta}_n}{\pi}} \cdots\cdots \left(\frac{\sqrt{-f} + \sqrt{\alpha_0}}{\sqrt{-f} - \sqrt{\alpha_0}} \right)^{\frac{\theta_0 - \bar{\theta}_1}{\pi}} \tag{2.12}$$

Now we can obtain (2.10) by allowing all the straightline segments in Fig.2.1 to form a smooth curve. However, it can be shown that (2.10) defines the complex velocity $u - iv$ as an analytic function of the complex potential $\phi + i\psi$, and satisfies

the required conditions for $\psi = 0$. That is

(1) $u - iv$ is real on $\psi = 0, \phi < -1$,

(2) $u - iv = R(\phi)e^{-i\Theta(\phi)}$ for $-1 \leq \phi \leq 0, \psi = 0$,

for some real function $R(\phi)$,

(3) $|u - iv| = 1$ for $\phi > 0, \psi = 0$,

(4) $u - iv \to 1$ as $\phi \to \pm\infty$.

Hence (2.10) satisfies $(2.8 - 2.9)$ when $g = 0$. Furthermore, (2.10) holds for bodies with discontinuous as well as continuous slope.

From (2.10) we can extract the free streamline slope as

$$\theta(\phi) = \frac{1}{\pi}\int_{-1}^{0} \Theta'(s)\arctan\left(\frac{2\sqrt{-\phi s}}{s+\phi}\right)ds. \tag{2.13}$$

As $\phi \to \infty$, $\theta(\phi)$ has the following form:

$$\theta(\phi) = \frac{1}{\sqrt{\phi}}\left(\frac{2}{\pi}\int_{-1}^{0} \Theta'(s)\sqrt{-s}ds\right) + O\left(\phi^{-3/2}\right). \tag{2.14}$$

The corresponding asymptotic form of the free streamline at a large distance downstream can be written as

$$y = y_0 + \sqrt{x}\left[\frac{2}{\pi}\int_{-1}^{0} \Theta'(s)\sqrt{-s}ds\right] + O(x^{-1/2}\log x), \tag{2.15}$$

where y_0 is a constant. The drag force F is given by

$$F = \frac{\rho}{\pi}\left[\int_{-1}^{0} \Theta'(s)\sqrt{-s}ds\right]^2. \tag{2.16}$$

where ρ is the fluid density.

In general, the free streamline is parabolic at a large distance downstream, and the draught is infinite. However, there is a special case when this is not so, and it is clear that the free streamline asymptotes to a line parallel to the x axis if the zero-drag condition,

$$\int_{-1}^{0} \Theta'(s)\sqrt{-s}ds = 0, \tag{2.17}$$

is satisfied by the specified body shape. Furthermore, we can verify that $y_0 = 0$ in this $g = 0$ case, by using (2.10),(2.17) and the Cauchy residue theorem in the complex plane. Thus the draught is zero in this special case; finite non-zero draught is impossible.

It should be emphasized that (2.17) is a necessary but not a sufficient condition for a physically acceptable shape of zero draught, since some profiles may cut themselves even though they satisfy (2.17). For bodies with discontinuous slopes (as in Fig.2.1), condition (2.17) should be written in the form

$$\int_{-1}^{0} \sqrt{-s}d\Theta = 0, \tag{2.18}$$

where the discontinuity at $\phi = -\alpha_j$ has the contribution $\sqrt{\alpha_j}(\bar{\theta}_{j+1} - \bar{\theta}_j)$. Under the zero-drag (consequently zero-draught) condition, equations (2.14) and (2.17) show that θ behaves like $\phi^{-3/2}$ as $\phi \to \infty$.

2.4 Numerical scheme for $g \neq 0$

To solve the integral equation (2.8) in the presence of gravity, introduce the N mesh points defining the free surface by

$$\varphi_i = i^2\Delta^2, \quad i = 0, 1, 2, 3, ..., N-1. \tag{2.19}$$

The quantity Δ^2 is a small parameter that controls the size of the intervals of discretization. Also, N corresponding unknowns are defined by θ_i, by the definition

$$\theta_i = \theta(\varphi_i), \quad i = 0, 1, 2, ..., (N-1). \tag{2.20}$$

The unknown θ_0 has the special property that it is the slope of the body at $\varphi = 0_-$ as well as that of the free-surface at $\varphi = 0_+$. Thus we are assuming that the free-surface joins the body smoothly and tangentially at $\phi = 0$, and in particular are excluding in this chapter the possibility that this point is a stagnation point. The problem with a stagnation point at attachment is treated in the next chapter.

We enforce the finite draught (and wave-free) requirement by assuming an asymptotic $\varphi^{-3/2}$ decay at infinity, by analogy with (2.14) subject to (2.17). Thus we set

$$\theta(\varphi) = \theta_{N-1}\left[\frac{(N-1)^2\Delta^2}{\varphi}\right]^{3/2}, \text{ for } \varphi > (N-1)^2\Delta^2. \tag{2.21}$$

Now $\tau(\phi)$ is computed at intermediate meshpoints

$$\phi_i = \begin{cases} (i-\frac{1}{2})^2\Delta^2, & \text{if } i \neq 1; \\ \frac{1}{2}\Delta^2, & \text{if } i = 1. \end{cases} \tag{2.22}$$

i.e. we evaluate

$$\tau_i = \tau(\phi_i), \quad i = 1, 2, 3, ..., N, \tag{2.23}$$

in terms of θ_i, by applying the trapezoidal rule to the integral (2.8), with the mesh points φ_i. The contribution to (2.8) for $\varphi > \varphi_{N-1}$ is estimated by the use of (2.21). N equations are obtained from (2.23) to evaluate $\theta_i = \theta_i(\varphi_i), i = 0, 1, 2, ..., (N-1)$, for any given function $\Theta(\phi)$.

When $g = 0$, (2.8) reduces to a system of linear equations, the solution of which agrees with the exact values to within 99% or better accuracy when $N = 50$ and $\Delta^2 = \frac{1}{600}$ and these values of N and Δ^2 were used for all calculations. Using solution at $g = 0$ as an initial guess, Newton's method seemed to converge very efficiently for a moderate value of gravity, $g = 1.0$ (say). This solution is now used as an initial guess to obtain the next solution, which corresponds to a higher gravity, $g = 2.0$, etc. This process of increasing gravity can be continued up to a certain upper limit g_m (say), as discussed in the next section. The profiles of the ship bow and of the free surface were obtained by numerically integrating (2.6) and

$$\frac{\partial x}{\partial \phi} = e^{-\tau} \cos\theta. \tag{2.24}$$

Some numerical results are given in the Tables 2.1, 2.2 and 2.3.

2.5 Discussion of results

Consider first a polygonal body defined by

$$\begin{aligned}\Theta(\phi) &= \theta_0, \quad -\alpha_0 < \phi < 0, \\ &= \bar{\theta}_1, \quad -\alpha_1 < \phi < -\alpha_0, \\ &= \bar{\theta}_2, \quad -\alpha_2 < \phi < -\alpha_1, \\ &= ... \\ &= ... \\ &= ... \\ &= \bar{\theta}_n, \quad -1 < \phi < -\alpha_{n-1}.\end{aligned} \tag{2.25}$$

Suppose first that $g = 0$. Substitute into the condition (2.18) to get

$$\bar{\theta}_n\sqrt{-1} + (\bar{\theta}_{n-1} - \bar{\theta}_n)\sqrt{\alpha_{n-1}} + ... + (\theta_0 - \bar{\theta}_1)\sqrt{\alpha_0} = 0, \tag{2.26}$$

which can be rewritten as

$$-\theta_0\sqrt{\alpha_0} = \bar{\theta}_n(1 - \sqrt{\alpha_{n-1}}) + \bar{\theta}_{n-1}(\sqrt{\alpha_{n-1}} - \sqrt{\alpha_{n-2}}) + ... + \bar{\theta}_1(\sqrt{\alpha_1} - \sqrt{\alpha_0}). \tag{2.27}$$

Now it is clear that, for all the body shapes which have $\bar{\theta}_i > 0$, $i = 1, 2, ..., n$, the value of θ_0 must be negative. These geometries have the property that the bow completely lies above its flat bottom level. When $g > 0$ the adopted numerical procedure determines the value of θ_0 for given $\bar{\theta}_1, ..., \bar{\theta}_n, \alpha_0, \alpha_1, ..., \alpha_{n-1}$, such that the corresponding bow flow is splashless.

By running the scheme for many different values of $\alpha_0, \alpha_1, ..., \alpha_{n-1}$, and $\bar{\theta}_1, ..., \bar{\theta}_n (\bar{\theta}_i > 0)$, it was observed that, as g increases from zero to some upper

limit g_m, θ_0 increases from the negative value given by (2.27) to some non-zero negative value θ_m (say), where $\theta_0 < \theta_m < 0$ for this particular class. As g approached g_m, Newton's method needed more iterations to converge to a solution, and finally it failed beyond $g = g_m$. Figures 2.2 and 2.3 show some simple polygonal profiles of this class. The upper bound g_m itself is not easy to estimate, but the largest values shown in Tables 2.1 and 2.2 are close to g_m.

Figure 2.4 corresponds to the smooth bow shape function $\Theta(\phi) = \theta_0 + (\theta_0 + k)\phi + k\phi^2$ in the same class, where k is a negative constant and $\Theta(0) = \theta_0$ is determined by the numerical scheme in order to yield a splashless solution for $g > 0$. At $g = 0$, by substituting $\Theta(\phi)$ into (2.17), we get the initial value $\theta_0 = k/5$, which is negative. Further, this function has the following properties:

$$\text{(i) } \Theta(\phi) > 0 \quad \text{for } -1 < \phi < -\left(\frac{\theta_0 + k}{2k}\right),$$

$$\text{(ii) } \Theta(\phi) < 0 \quad \text{for } -\left(\frac{\theta_0 + k}{2k}\right) < \phi < 0.$$

It is clear that the section (ii) with $\Theta(\phi) < 0$ describes a downward-directed rudder-like segment, analogous to the last straightline segment in the case of polygonal bodies. At $k = -25\pi/12$, it was observed that $g_m \approx 1.694$ was the upper bound for splashless solutions, and θ_0 increased from -1.32 at $g = 0$ to -0.495 at $g = g_m$. Smaller values of k produced higher values for the upper limit g_m. In Tables 2.1 and 2.2, exact upper bounds were not given, due to the fact that a very large number of computations is required to approach this number.

2.6. Concluding remarks

The bow shapes considered in this chapter have the special property that they lie entirely above the plane lower surface and the flow separates tangentially from the bow. The numerical evidence strongly suggests that this class will have no splash-free solutions without a downward-angled rudder-like segment at the extreme of the bow.

In fact, various attempts were made to obtain a solution without a downward-angled segment at the attachment, even considering the possibility of having a solution which may not belong to the above restricted class. However, no such cases were found, and the solutions with downward slope at attchment seem acceptable for a design of a waveless stern rather than a splashless bow.

Unequally spaced grid points in (2.19) and the selection of intermediate points in (2.22) increased the accuracy considerably when compared to trial runs using an uniform grid. Models were tested for many different values of N and Δ^2 but $N = 50$ and $\Delta^2 = \frac{1}{600}$ gave adequate accuracy. It should be emphasized that the suggested upper bound g_m for gravity varies according to the parameters that determine the bow geometry. In Fig.2.1 higher values of g_m are obtainable by lowering the oblique flat front. It is suggested that a theoretical proof may be feasible to verify the existence of such upper bounds for gravity, possibly by justifying that it is unlikely to have a tangential flow attachment at infinite gravity, i.e at zero Froude number.

Tables and figures

$\alpha_0 = .25, \theta_1 = \pi/6$		
g	θ_0	D
0	-0.5300	0.000
0.03	-0.5120	0.054
0.05	-0.5004	0.068
0.07	-0.4905	0.079
1.0	-0.2710	0.230
2.0	-0.1746	0.283
5.0	-0.0715	0.341
12.0	-0.0273	0.369
20.0	-0.0160	0.377

Table 2.1: Corresponds to Fig. 2.2

$\alpha_0 = .25, \theta_1 = \pi/2$		
g	θ_0	D
0	-1.590	0.000
0.05	-1.500	0.371
0.09	-1.440	0.481
0.3	-1.196	0.850
1.0	-0.555	0.872
1.3	-0.250	0.896
1.4	-0.080	0.930
1.5	-0.010	0.968

Table 2.2: Corresponds to Fig. 2.3

$k = -25\pi/12$		
g	θ_0	D
0	-1.324	0.000
0.05	-1.284	0.102
0.1	-1.255	0.142
0.2	-1.204	0.194
0.500	-1.076	0.305
1.000	-0.890	0.443
1.600	-0.609	0.610
1.694	-0.495	0.664

Table 2.3: Corresponds to Fig. 2.4

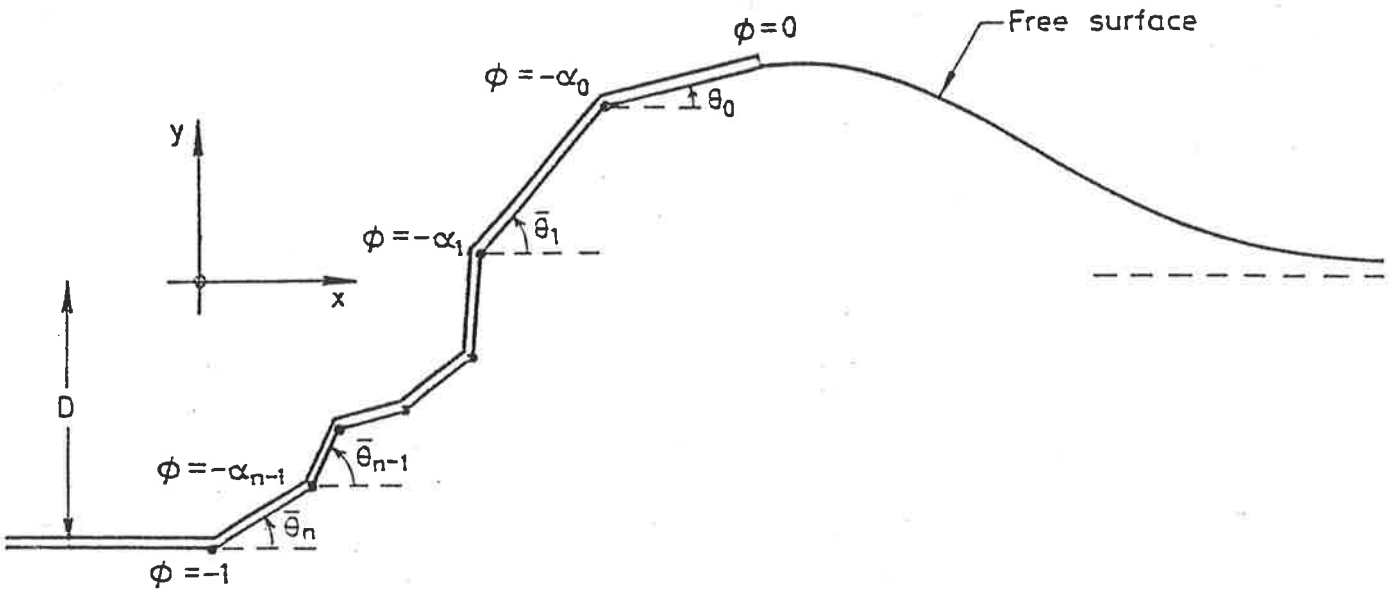

Figure 2.1. Sketch of a flow past a semi-infinite body (polygonal) with a smooth detachment.

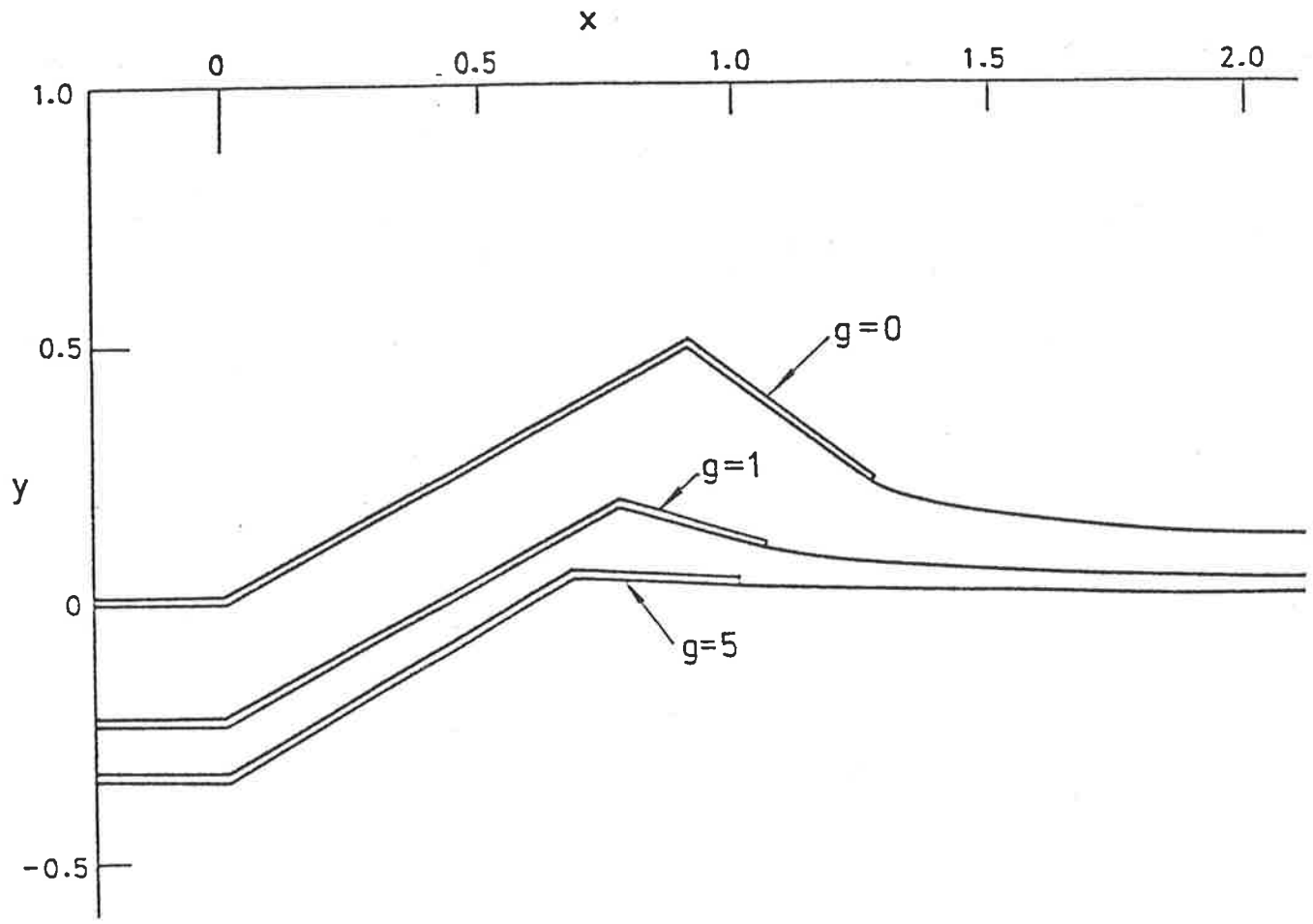

Figure 2.2. Bow with a plane oblique front and a downward angled end segment.

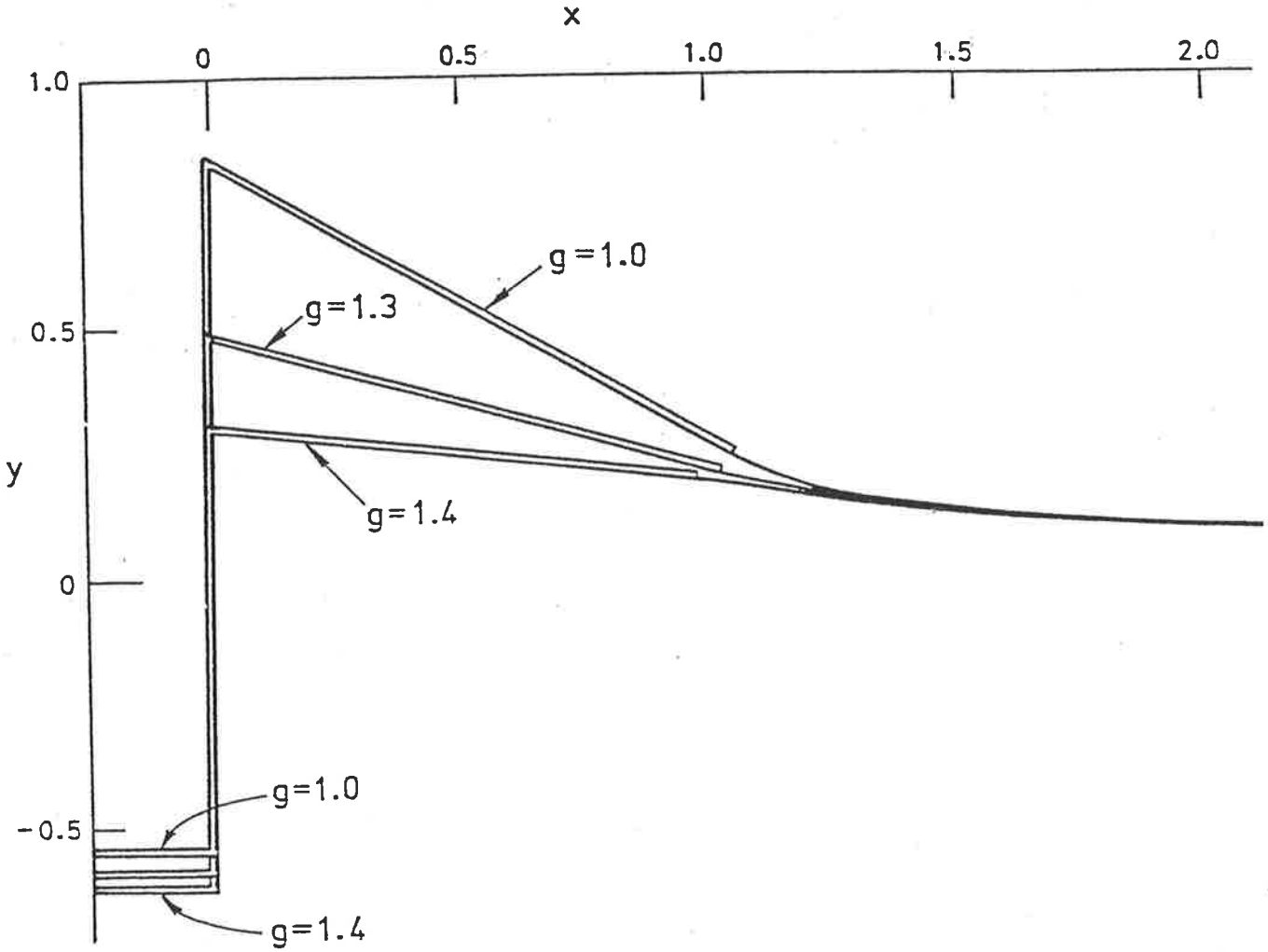

Figure 2.3. Bow with a plane vertical front and a downward angled end segment.

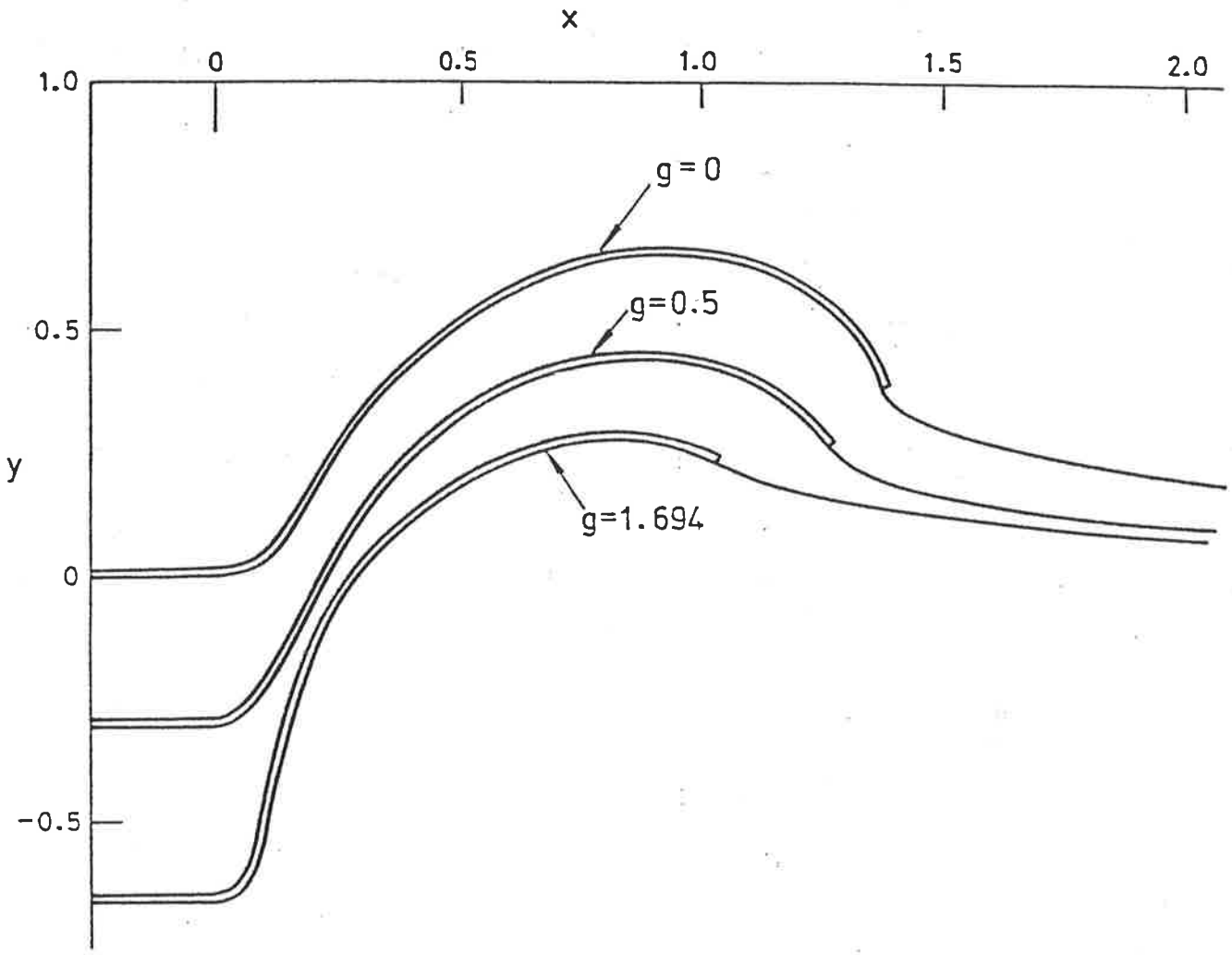

Figure 2.4. Smooth bow $\Theta(\phi) = \theta_0 + (\theta_0 + k)\phi + k\phi^2$ at $k = -25\pi/12$.

CHAPTER 3

SPLASHLESS SHIP BOWS WITH STAGNANT ATTACHMENT

3.1 Introduction

The main results on splashless and wave-free bows to be presented in this chapter, involve conventional-type bulbous bows with a stagnation point at attachment. The problem is treated in the same two dimensional frame work as in the previous chapters. It is proved that such a splashless flow has a locally horizontal free surface at attachment, if the angle to the horizontal of the body at the stagnation point is greater than 60^0. A numerical scheme very similar to that previously discussed is then employed to obtain splashless solutions, by allowing the scheme to change the body geometry accordingly.

Numerical evidence suggests that wave-free stern flows, or equivalently splash-free bow flows, demand underwater bodies of a unique bulbous shape for $F > 0.54$, where F is the Froude number based on the draught of the ship. For $0.5 < F < 0.54$, this unique shape is non-bulbous and essentially rectangular. For $0.45 < F < 0.5$ there seems to exist two or three distinct solutions and consequently two or three quite different bulb sizes that allow splash-free flows, and for $F < 0.45$, many solutions exist. The existence of many solutions for small Froude numbers ($F < 0.45$) supports the conclusion that the body geometry becomes arbitrary in this range, in which gravity is effectively infinity and no stern creates waves.

A large collection of results is included, generalising the single case presented by Tuck and Vanden-Broeck[2]. In particular, variation in the bulb shape and size with Froude number is discussed in detail.

3.2 Formulation

Consider the steady two-dimensional irrotational flow of an inviscid incompressible fluid past a semi-infinite stern-like body, whose lower surface $y^* = -D^*$, $x^* < 0$ is plane (See Fig 3.1). As $x^* \to -\infty$, the velocity underneath the body is assumed to approach the constant value U. On the other hand, when $x^* > 0$, the level $y^* = 0$ corresponds to the level of the free surface at which the velocity is equal to U; thus, in general, we expect a mean free-surface level $y^* = 0$ as $x^* \to +\infty$, and can interpret D^* as the "draught" of the body. It is assumed that the flow rises up the rear face of the body to a stagnation point S, at which separation occurs.

Denote the potential function by ϕ^*, and the stream function by ψ^*, and choose $\phi^* = 0$ at the stagnation point and $\psi^* = 0$ on the free surface and on the surface of the body. The value of ϕ^* at $x^* = 0$, $y^* = -D^*$ is denoted by $-K$ and the body has non-trivial shape variation only in $-K < \phi^* < 0$. Define $u^* - iv^*$ as an analytic function of the complex potential $f^* = \phi^* + i\psi^*$, where u^*,v^* are the velocity components in the x^* and y^* directions respectively. These variables are now made dimensionless by referring them to the velocity scale U and the length scale K/U. Thus we can introduce the new dimensionless variables

$$x + iy = (x^* + iy^*).U/K, \tag{3.1}$$

$$u - iv = (u^* - iv^*)/U, \tag{3.2}$$

$$f = \phi + i\psi = f^*/K = (\phi^* + i\psi^*)/K. \tag{3.3}$$

The function $\tau - i\theta$ defined by

$$\frac{df}{dz} = u - iv = \exp(\tau - i\theta). \tag{3.4}$$

is an analytic function of $f = \phi + i\psi$ in the half plane $\psi \leq 0$, and tends to zero as $|f| \to \infty, \psi \leq 0$. Therefore, on $\psi = 0$, its real part is the Hilbert transform of its imaginary part, and we have

$$\tau(\phi) = \frac{1}{\pi} \int_{-\infty}^{+\infty} \frac{\theta(\varphi)}{\varphi - \phi} d\varphi. \tag{3.5}$$

Here $\tau(\phi)$ and $\theta(\phi)$ denote respectively $\tau(\phi, 0_-)$ and $\theta(\phi, 0_-)$. The integral in (3.5) is to be interpreted in the Cauchy principal-value sense. The kinematic condition on the body yields

$$\theta = 0, \qquad \psi = 0, \phi < -1, \tag{3.6}$$

$$\theta = \Theta(\phi), \quad \psi = 0, -1 < \phi < 0. \tag{3.7}$$

Here the function $\Theta(\phi)$ defines the shape of the body. For the sake of convenience, a straightline segment is introduced at the extreme of the body by setting

$$\Theta(\phi) = \beta \qquad \text{for } -b \leq \phi < 0, \tag{3.8}$$

where β is the slope of this segment and $-1 < -b < 0$ (See Fig.3.1). Bernoulli's equation and the condition of constant pressure on the free surface yield

$$\gamma y + \frac{1}{2} q^2 = \frac{1}{2}, \tag{3.9}$$

where

$$\gamma = gK/U^3, \tag{3.10}$$

and y is given by

$$\frac{\partial y}{\partial \phi} = e^{-\tau} \sin\theta. \tag{3.11}$$

Differentiating (3.9) with respect to ϕ, using (3.11), and integrating gives

$$\gamma \int_{\infty}^{\phi} \sin\theta d\varphi + \frac{1}{3} e^{3\tau} = \frac{1}{3}, \tag{3.12}$$

and

$$\tau(\phi) = \frac{1}{3} \log[1 - 3\gamma \int_{\infty}^{\phi} \sin\theta d\varphi] \quad \text{for } \phi > 0, \tag{3.13}$$

where the limits $y \to 0$ and $\tau \to 0$ as $\phi \to \infty$ have been enforced. Substituting (3.6), (3.7) and (3.13) into (3.5), we get

$$\int_0^{\infty} \frac{\theta(\varphi)}{\varphi - \phi} d\varphi + T(\phi) = \frac{\pi}{3} \log[1 - 3\gamma \int_{\infty}^{\phi} \sin\theta(\varphi) d\varphi] \quad \text{for } \phi > 0, \tag{3.14}$$

where

$$T(\phi) = \int_{-1}^{0} \frac{\Theta(\varphi)}{\varphi - \phi} d\varphi = \int_{-1}^{-b} \frac{\Theta(\varphi)}{\varphi - \phi} d\varphi + \beta \log|\frac{\phi}{\phi + b}|. \tag{3.15}$$

$T(\phi)$ is a known function, for a given bow-shape function $\Theta(\phi)$.

For given $\Theta(\phi), -1 \leq \phi \leq 0$, the problem reduces to finding a function $\theta(\phi)$ satisfying the nonlinear integral equation (3.14) for $\phi > 0$. The Froude number based on draught is defined by

$$F = \frac{U}{\sqrt{gD^*}} = \frac{1}{\sqrt{\gamma D}}, \tag{3.16}$$

where D is the draught in the dimensionless scale, i.e $D = UD^*/K$.

3.3 Nature of the solutions

Since the fluid is stagnant at $\phi = 0$, it is clear from (3.4) and (3.13) that as $\phi \to 0^+, \tau \to -\infty$, and hence the right hand side of (3.14) is singular for $\phi \to 0^+$. On the free streamline, in the vicinity of the stagnation point we may assume

$$\theta(\phi) = -\theta_0 + k\phi^n \quad \text{for} \quad 0 \leq \phi < \delta, \tag{3.17}$$

where $\theta(0^+) = -\theta_0$, k, n are constants with $n > 0$ and δ is a sufficiently small positive quantity. Substituting (3.15), (3.17) into (3.14) and re-writing (3.14) we have

$$1 - 3\gamma \int_{\infty}^{\phi} \sin\theta d\varphi = \left(\frac{\phi}{\phi + b}\right)^{\frac{3\beta}{\pi}} \left(\frac{\phi + \delta}{\phi}\right)^{\frac{-3\theta_0}{\pi}} \exp[S(\phi)], \tag{3.18}$$

where

$$S(\phi) = \int_{-1}^{-b} \frac{\Theta(\varphi)}{\varphi - \phi} d\varphi + \int_{0+}^{\delta} \frac{k\varphi}{\varphi - \phi} d\varphi + \int_{\delta}^{\infty} \frac{\theta(\varphi)}{\varphi - \phi} d\varphi. \tag{3.19}$$

It is clear that $S(\phi)$ is a well behaved function for $0 \leq \phi < \delta$ and, in the limit as $\phi \to 0^+$, (3.18) can be written in the form

$$-3\gamma \sin\theta_0 = \frac{d}{d\phi}\left[\frac{\phi^{3(\beta+\theta_0)/\pi}(\phi + \delta)^{-3\theta_0/\pi} \exp[S(\phi)]}{(\phi + b)^{3\beta/\pi}}\right]. \tag{3.20}$$

This limit for θ_0 exists and is finite only for $\beta + \theta_0 \geq \frac{\pi}{3}$, and further it is clear that $\theta_0 = 0$ if $\beta + \theta_0 > \frac{\pi}{3}$, in order to satisfy (3.20). In other words, solutions may exist in only one or other of the following two categories,

$$\text{(i)} \quad \beta > \frac{\pi}{3}, \qquad \text{with} \quad \theta_0 = 0, \tag{3.21}$$

$$\text{(ii)} \quad \beta + \theta_0 = \frac{\pi}{3}, \qquad \text{if} \quad \beta < \frac{\pi}{3}. \tag{3.22}$$

The solutions for the "nearly horizontal entrance" case (ii), in which the inclination β of the flat front segment is less than 60^0 and the angle between the body and the streamline is 120^0 at the stagnation point, are not presented in this research. The resulting bow geometries are non-bulbous, but of little practical relevance. It appears that any given underwater shape with an entrance satisfying $\beta < \pi/3$ can be splashless at some (to-be-determined) Froude number . Equivalently, any given specification $\Theta(\phi), -1 < \phi < -b$ of the underwater shape can be combined with a flat sloping entrance having a unique (to-be-determined) angle $\beta < \pi/3$, to yield a splashless flow at any given Froude number. If the given Froude number is reasonably large, as corresponds to practical cases, the required entrance angle β is quite small (i.e. the body is nearly horizontal at attachment), and the resulting bow shape is unrealistic. On the other hand, if the given Froude number is small, the required entrance angle β approaches $\pi/3$ from below.

It is interesting to investigate this low Froude number limit in general by approximating equation (3.14), i.e. by assuming $\theta(\phi) = \bar{\theta}(\phi)/\gamma$, for some bounded $\bar{\theta}(\phi)$ and letting $\gamma \to \infty$. Thus, we have solutions for very large γ given by

$$\theta(\phi) = -\frac{1}{3\gamma}\frac{d}{d\phi}\left[\left(\frac{\phi}{\phi+b}\right)^{\frac{3\beta}{\pi}} \exp\left(\frac{3}{\pi}\int_{-1}^{-b}\frac{\Theta(\varphi)}{\varphi-\phi}d\varphi\right)\right] \quad \text{for} \quad \phi > 0, \qquad (3.23)$$

Although (3.23) was derived irrespective of the value of β, it predicts an unacceptable singularity at $\phi = 0^+$ unless $\beta \geq \pi/3$. In case (ii) above, this confirms that the only acceptable possibility as $\gamma \to \infty$ is that β approaches $\pi/3$ from below. Furthermore, it is evident from (3.23) that, in case (i) where $\beta > \pi/3$, we do not need any specific bow geometry near zero Froude number in order to

yield a splashless solution. In other words, this conclusion supports the physically obvious fact that flow around a semi-infinite body of arbitrary geometry creates no waves at infinite gravity. Also, one can verify easily the fact that the draught approaches a constant value as $\gamma \to \infty$.

Solutions for the "nearly vertical entrance" case (i), with $\beta > \pi/3$, in general demand bodies of a bulbous nature, i.e. have $\Theta > \pi/2$ for some ϕ values, at finite γ. In the next section, a numerical scheme is presented to explore these solutions at $\beta = \pi/2$, i.e for a vertical face at the waterline, by setting

$$\Theta(\phi) = \begin{cases} \pi/2, & -b \leq \phi < 0; \\ A(\phi+1)(\phi+b) + \frac{\pi(\phi+1)}{2(1-b)}, & -1 < \phi \leq -b. \end{cases} \tag{3.24}$$

Thus (3.24) defines a continuous slope for the non-trivial section of the body, and the constant A is to be determined in order to satisfy the integral equation (3.14) for fixed b. Tuck and Vanden-Broeck[2] used the same one-parameter function for $\Theta(\phi)$, and they found that a train of waves is present on the free surface in general. Further, they succeeded in their scan for a particular unique value of the parameter A, for which the free surface had zero wave amplitude. In the present study, the numerical technique allows us to investigate the entire range of possible values for A, by restricting attention only to waveless solutions. Substituting (3.15) and (3.24) into (3.14) and rewriting (3.14) we get

$$1 - 3\gamma \int_{\infty}^{\phi} \sin\theta d\varphi = \left(\frac{\phi}{\phi+b}\right)^{3/2} \exp\left[\frac{3}{\pi}\left(T_1(\phi) + AT_0(\phi) + \int_0^{\infty} \frac{\theta(\phi)}{\varphi - \phi} d\varphi\right)\right], \tag{3.25}$$

where

$$T_1 = \frac{\pi}{2}\left[1 + \left(\frac{1+\phi}{1-b}\right)\log\left(\frac{\phi+b}{\phi+1}\right)\right], \tag{3.26}$$

and

$$T_0(\phi) = (\phi+1)(\phi+b)\log\left(\frac{\phi+b}{\phi+1}\right) + \phi(1-b) + \frac{1}{2}(1-b^2). \tag{3.27}$$

Now it is clear from (3.25), (3.26) and (3.27) that $T_1(\phi), T_0(\phi)$, and $\int_0^\infty \frac{\theta(\varphi)}{\varphi-\phi}d\varphi$ tend to constants as $\phi \to 0^+$, subject to the condition $\theta(0^+) = 0$. Further, these three functions tend to zero at the rate ϕ^{-1} as $\phi \to +\infty$. Therefore, by differentiating (3.25) and observing the nature of $\sin\theta$ at these extremes, we can conclude that $\theta(\phi)$ behaves like $\phi^{1/2}$ and ϕ^{-2} (more generally $\phi^{\frac{3\beta}{\pi}-1}$ and ϕ^{-2}) as ϕ tends to 0^+ and $+\infty$ respectively.

3.4 Numerical scheme

To solve the integral equation (3.25) subject to the restriction $\theta(0^+) = 0$, introduce the N mesh points defining the free surface by

$$\varphi_i = i^2\Delta^2, \quad i = 1, 2, 3, ..., N-1. \tag{3.28}$$

The small parameter Δ^2 controls the size of the interval of discretization. Also, N corresponding unknowns θ_i are defined by

$$\theta_i = \theta(\varphi_i), \quad i = 1, 2, ..., (N-1), \tag{3.29}$$

$$\theta_N = A. \tag{3.30}$$

The unknown θ_N or A has the special property that it is a parameter that uniquely identifies the slope of the body at any fixed b and γ.

The wave-free requirement is enforced by assuming an asymptotic φ^{-2} decay at infinity. Thus we set

$$\theta(\varphi) = \theta_{N-1}\left[\frac{(N-1)^2\Delta^2}{\varphi}\right]^2, \text{ for } \varphi > (N-1)^2\Delta^2. \tag{3.31}$$

Further, for better numerical accuracy we may assume

$$\theta(\varphi) = \theta_1\sqrt{\varphi/\Delta^2}, \quad \text{for } 0 \le \varphi \le \varphi_1 = \Delta^2, \tag{3.32}$$

in the first interval.

Redefine (3.25) at $\phi = \phi_i$ as

$$Z_i = 1 + 3\gamma\int_{\phi_i}^{\infty} \sin\theta - \left(\frac{\phi_i}{\phi_i + b}\right)^{\frac{3}{2}} \exp\left[\frac{3}{\pi}\left(T_1(\phi_i) + AT_0(\phi_i) + \int_0^{\infty}\frac{\theta(\varphi)}{\varphi - \phi_i}d\varphi\right)\right], \tag{3.33}$$

where

$$\phi_i = \begin{cases} (i-\frac{1}{2})^2\Delta^2, & \text{if } i \neq 1; \\ \frac{1}{2}\Delta^2, & \text{if } i = 1. \end{cases} \tag{3.34}$$

By applying the trapezoidal rule to (3.33) with the mesh points φ_i, the quantity Z_i is computed in terms of θ_i at the intermediate mesh points defined by (3.34). The contribution to Z_i for $\varphi > \varphi_{N-1}$ and $\varphi < \varphi_1$ is estimated by the use of (3.31) and (3.32) respectively. It should be noted that for $i \geq 2$

$$\begin{aligned} \int_{\phi_i}^{\infty} \sin\theta d\varphi &= \int_{(i-\frac{1}{2})^2\Delta^2}^{i^2\Delta^2} \sin\theta d\varphi + \int_{i^2\Delta}^{\infty} \sin\theta d\varphi \\ &= R_i[\sin\theta_{i-1} + \sin\theta_i]\left(\frac{\varphi_i - \varphi_{i-1}}{2}\right) + \int_{i^2\Delta^2}^{\infty} \sin\theta d\varphi, \end{aligned} \tag{3.35}$$

where the weights $R_i(\approx .5)$ are estimated by

$$R_i = \frac{i^2 - (i-\frac{1}{2})^2}{i^2 - (i-1)^2}, \qquad 2 \leq i \leq N. \tag{3.36}$$

N equations ($Z_i = 0, i = 1, 2, 3, ...N$) are obtained from (3.33) to evaluate $\theta_i = \theta_{(\varphi_i)}, i = 1, 2, 3, ...(N-1), \theta_N = A$ for a given slope function $\Theta(\phi)$, which contains an unknown parameter A.

This system of N non-linear equations was solved by using Newton's method. First, the vertical section of the bow was controlled by fixing the value of b, and then, for a good initial guess of $\theta_i (i = 1, 2, ...N)$ with an input value of γ greater than 2.0, the method always converged to a solution. The output value of A was always found to be negative and, with the same values of b and γ but for a different initial guess of θ_i, a finite number (usually 2 or 3) of distinct solutions could be obtained. In each case, by using the known solution as the initial guess, the next

solution was obtained for a slightly different γ. This procedure allows us to obtain multiple solutions for a wide range of γ values and to investigate the variation of this unknown body parameter $\theta_N = A(\gamma)$. The profiles of the ship bow and of the free surface were obtained by numerically integrating (3.11) and

$$\frac{\partial x}{\partial \phi} = e^{-\tau} \cos\theta. \tag{3.37}$$

3.5 Discussion of results

The splashless solution for the unknown parameter A in the bow shape function (3.24) is always negative (see Figs.3.2.a and 3.2.b). This indicates that the slope increases from $\Theta(-1) = 0$ to a maximum slope of $\Theta(\phi_m) = \Theta_{max}$(say), which is given by (3.24) at $\phi = \phi_m$, where

$$\phi_m = -\frac{1}{2}(1+b) - \frac{\pi}{4A(1-b)}. \tag{3.38}$$

It can be seen that $\Theta_{max} > \pi/2$ and that for $\phi > \phi_m$, $\Theta(\phi)$ decreases. Since $\Theta(-b) = \pi/2$, this shows that these profiles are of bulbous nature. As can be seen from Figures 3.2.a and 3.2.b, smaller values of γ produce higher values of $-A$ and consequently, higher values for Θ_{max}.(Note that Θ_{max} is an explicit function of A). On the other hand, larger values of γ (i.e. smaller values of $-A$) produce profiles with Θ_{max} closer to $\pi/2$. Three distinct families of solutions, denoted by C_1, C_2 and C_3, were obtained for $-A(\gamma)$ at $b = .3$ (Fig.3.2.a) and the corresponding profiles are given in Figures 3.3,3.4 and 3.5 respectively, on the $x/D, y/D$ scale. Figure 3.2.b shows similar families corresponding to change of the input parameter b from 0.3 to 0.2, which creates a shorter vertical segment in the bow geometry (Figs. 3.6, 3.7, 3.8). These bulbous-character profiles have the following varying characteristics along each curve in Figures 3.2.a and 3.2.b.

(a) The profile is non-physical (i.e. cuts itself) for $-A > N_1$, where N_1 is positive.

(b) The profile is physically acceptable, but non-practical for $N_1 > -A > N_2 > 0$, because its maximum slope Θ_{max} is greater than 180^0.

(c) The profile is practical and has a bulbous geometry with $\Theta_{max} < 180^0$ for $-A < N_2$, where N_2 must be obtained by solving (3.24) for $\Theta(\phi_{max}) = \pi$.

Since the maximum angle Θ_{max} of the underwater geometry is an explicit function of the parameter A, a more physically meaningful representation of our solutions is to plot Θ_{max} versus the basic input parameter γ. Such a plot is given in same figures (3.2.a, 3.2.b) by adding an extra vertical axis which clearly shows the horizontal line $\Theta_{max} = 180^0$, below which solutions are practically useful for ship designs.

Another important quantity is the ratio (B/D) of the protrusion of the bulb to the draught. The protrusion B (Fig.3.1)is measured relative to the vertical segment. Figures 3.9.a and 3.9.b indicate the Froude number variation for each of the families C_1, C_2, C_3 and also give the protrusion of the bulb at several points along the curves. Figures 3.10.a and 3.10.b show the variation of the bulb size (relative protrusion as defined above) versus the Froude number F.

The program was able to recover three distinct families of solutions at fixed b for $\gamma < 4$. Above this value of γ, the draught-based Froude number is small ($F < 0.45$) and these solutions were not distinguishable. It is likely that more solutions than those belonging to the families C_1, C_2, C_3 also exist in this range. Along each curve in Figures 3.2.a and 3.2.b, as γ increases $-A$ decreases and finally, solutions for large γ (i.e low-Froude-number solutions) have a low value of $-A$. Consequently Θ_{max} is close to $\pi/2$ and the resulting profiles have nearly vertical geometries with a smooth rounded corner joining the flat bottom. At the

other extreme, very low γ (i.e. high F) solutions were not attempted, since $-A$ becomes very large (consequently Θ_{max} exceeds π) and the resulting profiles are non-physical for some $-A > N_1$, as mentioned above(see Figs. 3.2.a, 3.2.b).

The multiple solutions at any fixed γ all have different geometries, different draughts and hence different Froude numbers. For example, at $\gamma = 2.7$ with $b = .3$ we have three solutions with $-A = 7.01, 15.56, 19.75$ belonging to C_1, C_2 and C_3, with Froude numbers $0.548, 0.465$ and 0.454 respectively. The solution in C_3 is non-physical (i.e. cuts itself), the solution in C_2 is non-practical (i.e. $\Theta_{max} > \pi$) but the solution in C_1 is practical.

Let us now investigate these multiple solutions from a practical point of view, by assuming that the Froude number is given and we are asked to find suitable splash-free bow geometries. We can easily see from Figures 3.9.a and 3.9.b that there is a unique splashless member for $F > 0.54$ and this is in family C_1. The lowest Froude number in this family is about 0.54 and the highest is about 0.75. As we attempt to approach the higher Froude number solutions in family C_1 (i.e. $F > 0.72$), the program begins to produce numerically unstable and highly inaccurate solutions and finally does not converge to any solution.

The important family C_1 produces a unique splashless bulbous geometry with $0.75 > F > 0.54$, with the following characteristics. At the obtainable higher limit of F, we have a very sharp long bulb, and as F decreases, the sharpness gradually reduces (see Figs. 3.10.a, 3.10.b) until at around $F = 0.54$ the profile is nearly non-bulbous, with a flat front joining the flat ship bottom with a smooth rounded corner.

This family C_1 is always incomplete at the low-Froude-number end, since as we approach the lower limit of F (i.e. as we increase γ), the program reaches a point beyond which it fails to converge to further solutions of this family, and instead jumps to more numerically stable, but less useful solutions, in the family C_2 or C_3. In other words, this instability occurs when the uniqueness of splashless solutions fails. But none of these solutions produced profiles with F between 0.54 and 0.50; instead the multiple solutions (usually 2 or 3) obtained in family C_2 or C_3 have the property that the Froude number is between 0.50 and 0.45. Furthermore, these solutions in C_2 or C_3 have the special property that at fixed F with $0.45 < F < 0.50$, one profile can be nearly non-bulbous while the others can have a very sharp bulb.

For $F < 0.45$, we do not need any specific bulbous geometry in order to be splash-free, as is numerically evident by the apparent existence of more solutions than those belonging to C_2 or C_3, and by the fact that the bow geometry is arbitrary at zero Froude number.

Based on the above discussion on physical properties of the solutions of family C_1, we may come to the conclusion that the lowest Froude number for which a bulb is required in order to be splash-free is just around $F = 0.54$. These profiles can be produced in family C_1 only and further attention is given only to these solutions in Figures 3.11.a and 3.11.b, where the input parameter b which controls the length of the vertical flat front in the bow geometry is changed. Solutions of family C_1 only are plotted (B/D and Θ_{max}) against the Froude number.

The program was run for several different input values of b in the range $0.1 < b < 0.5$. Standard accuracy tests (doubling the number of points etc.) indicated good accuracy for $b > 0.2$, but not such good accuracy for $b \leq 0.2$. Some very accurate data are listed in Tables 3.1, 3.2 and 3.3 at $b = .3$ corresponding to the three families C_1, C_2 and C_3 respectively. $N = 60$ and $\Delta^2 = \frac{1}{150}$ were used for all the calculations. Higher values of b ($b > .5$) are not suitable for a design of a splashless ship bow, since the bulb becomes very sharp and the profiles tend to cut themselves before any practically-useful high Froude number is achieved. Vanden-Broeck and Tuck[6] obtained the splashless solution $A = -14.02$ at $\gamma = 1.0, b = 0.2$. This profile is approximated here on C_1 with $-A = 12.01$ at $\gamma = 1.0$. It was impossible to carry out a good accuracy test (doubling the number of points etc.) at this point due to the fact the Froude number is very high and the solution is neither sufficiently accurate nor numerically stable (see Fig.3.2.b).

3.6 Concluding remarks

The bow shapes considered in this research have the special property that they lie entirely above the plane lower surface and are of a single parameter family. This restriction can be removed by introducing one additional unknown body parameter. One can also use more complicated families, and introduce discontinuous slope at the point where the vertical front meets the bulb, as is seen in conventional-type bulbous bows. These corners will have either zero or infinite fluid velocities (i.e. $\tau = \pm\infty$) and consequently higher numerical errors in obtaining x and y coordinates. Equation (3.14) is not directly solvable numerically, due to the presence of a $\log|0|$ type singularity at the stagnation point, and this difficulty was completely avoided in (3.25). Unequally spaced grid points in (3.28) and the selection of the intermediate mesh points in (3.34) were recommended to be highly accurate by Tuck and the present author[6] in their research.

The one-parameter family of bow shapes considered here seems to have a unique splashless member for Froude numbers based on draught greater than 0.54 (see Fig. 3.8.a). (A super tanker normally operates above this limit.) A ship operating below this limit does not need to have a bulb to eliminate splashes. For $F < 0.50$, one can select 2 or 3 different bulb shapes, and for $F < 0.45$, there exist many solutions. Ultimately, as $F \to 0$ these shapes become indistinguishable, convincing us of the fact that the bow geometry is arbitrary as F tends to zero.

Existence of an upper bound for the Froude number is not confirmed in this research, because one may be able to obtain higher values by considering more

complicated bow geometries as suggested above. However, any solutions one may obtain at very high Froude number ($F > .72$) are likely to have very sharp bulbs and will not be important for ship designers.

At this writing, and in summary, it appears that, while wave making and breaking is a large component of the ship's expanded power, it is possible to greatly reduce the expanded power and to effectively cancel it in specific situations such as for very bluff barge-like bows where two dimensional solutions are highly appropriate.

Tables and figures

γ	$-A$	Θ_{max}	F	$B/D\%$
1.4	13.11	142.6	0.742	22.0
1.5	12.43	138.6	0.721	19.8
1.6	11.80	134.5	0.700	18.1
1.7	11.42	131.5	0.681	16.7
1.8	11.02	128.9	0.624	15.5
1.9	10.85	127.8	0.640	14.9
2.0	10.74	126.7	0.595	14.4
2.1	10.24	123.9	0.586	13.1
2.2	9.05	116.5	0.572	10.0
2.4	8.65	114.0	0.564	8.9
2.5	8.29	111.4	0.557	7.8
2.6	7.62	107.9	0.552	6.3
2.7	7.01	104.5	0.548	5.0
2.8	6.77	103.2	0.545	4.4

Table 3.1:Corresponds to Class C_1 at $b = .3$.

γ	$-A$	Θ_{max}	F	$B/D\%$
2.4	19.98	188.9	0.463	36.9
2.5	18.67	180.0	0.462	33.6
2.6	17.14	169.5	0.463	29.8
2.7	15.56	158.8	0.465	25.8
2.8	13.98	148.3	0.469	21.9
2.9	12.40	137.8	0.473	17.9
3.0	10.89	128.0	0.478	14.1
3.1	9.60	119.8	0.482	10.9
3.2	8.66	114.1	0.483	8.6
3.3	8.14	111.0	0.480	7.3
3.4	7.78	108.9	0.477	6.5
3.5	7.14	105.2	0.476	5.8
3.6	6.27	100.5	0.478	3.3
3.7	5.31	95.8	0.482	1.6
3.8	4.25	91.8	0.488	.3
3.9	2.92	90.0	0.502	0.0

Table 3.2:Corresponds to Class C_2 at $b = .3$.

γ	$-A$	Θ_{max}	F	$B/D\%$
2.7	19.75	187.2^0	0.454	35.9
2.8	18.13	176.2^0	0.455	31.9
2.9	16.55	165.5^0	0.457	28.1
3.0	15.06	155.5^0	0.459	24.4
3.1	13.72	146.5^0	0.462	21.0
3.2	12.61	139.2^0	0.462	18.3
3.3	11.95	134.9^0	0.460	16.6
3.4	11.72	133.4^0	0.454	16.0
3.5	11.28	130.5^0	0.450	14.8
3.6	10.54	125.8^0	0.450	13.0
3.7	9.66	120.2^0	0.454	10.8
3.8	8.72	144.4^0	0.453	8.6
3.9	7.77	108.8^0	0.455	6.4
4.0	6.83	103.5^0	0.458	4.4
4.1	5.93	98.9^0	0.462	2.6
4.2	5.09	94.9^0	0.465	1.2
4.3	4.35	92.1^0	0.467	0.4
4.5	3.32	90.0^0	0.468	0.0

Table 3.3:Corresponds to Class C_3 at $b = .3$

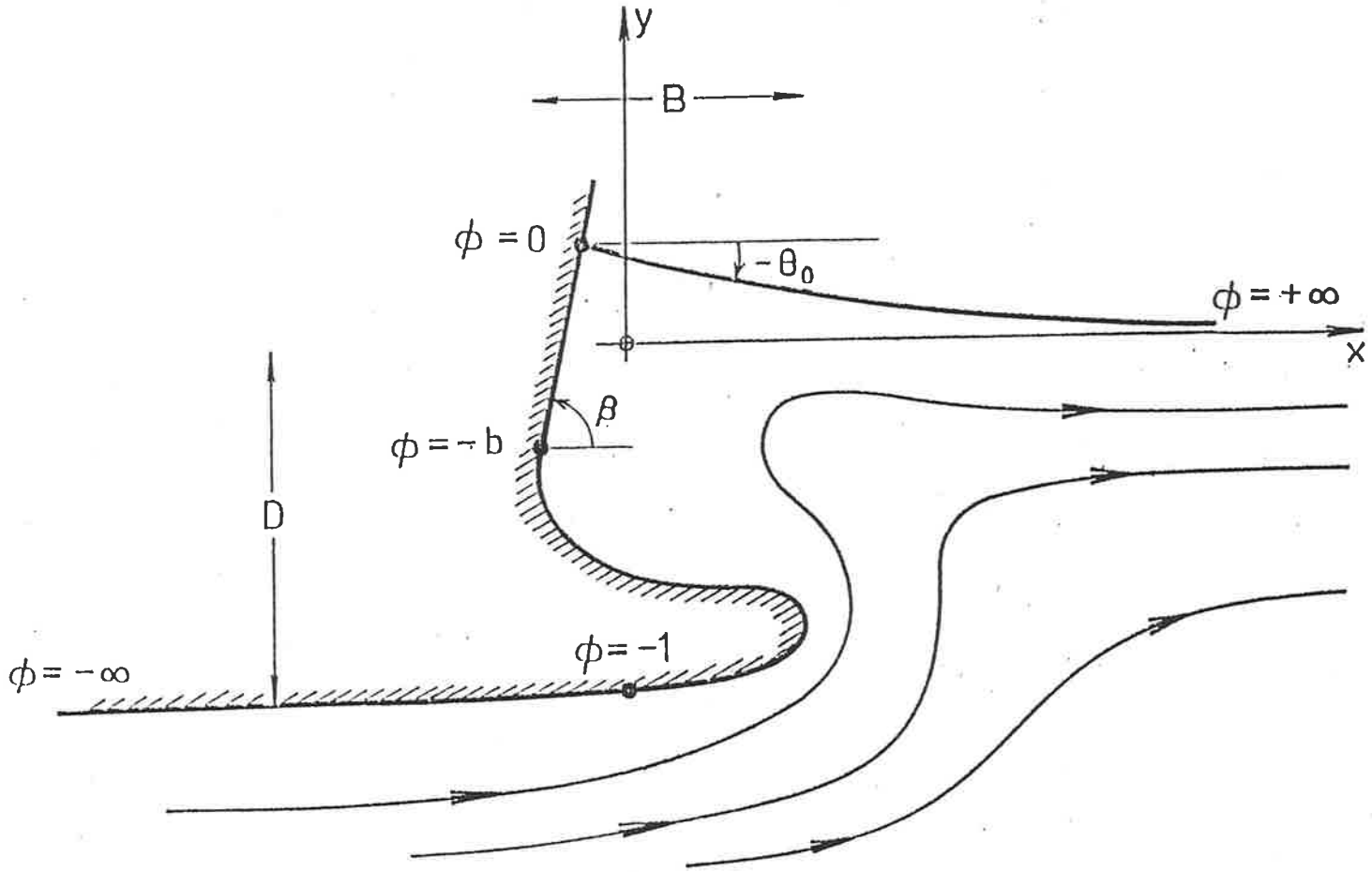

Figure 3.1: Sketch of a flow past a semi-infinite bulbous stern-like body.

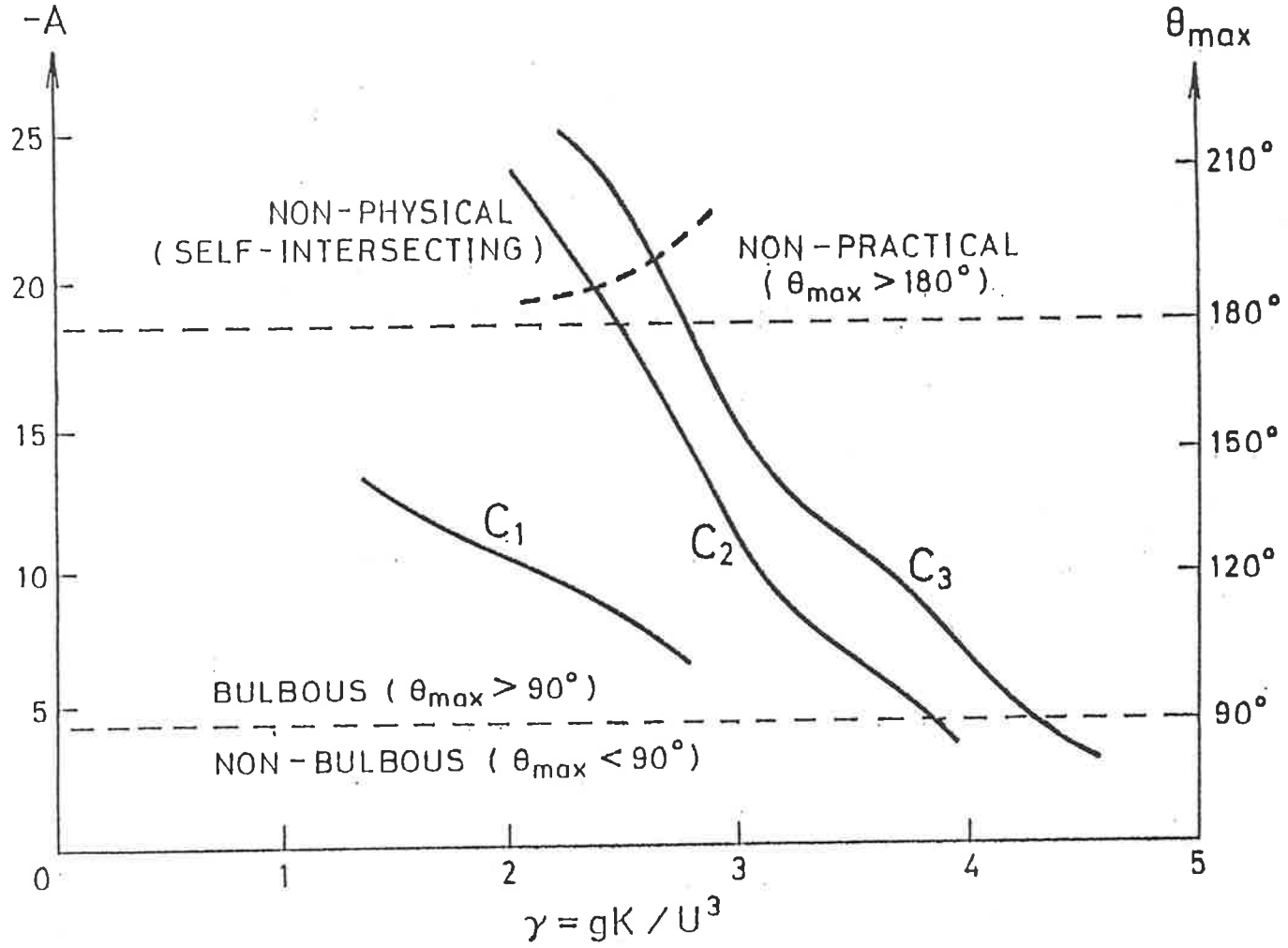

Figure 3.2.a: Variation of the body parameter A(or Θ_{max}) vs. γ at $b = .3$.

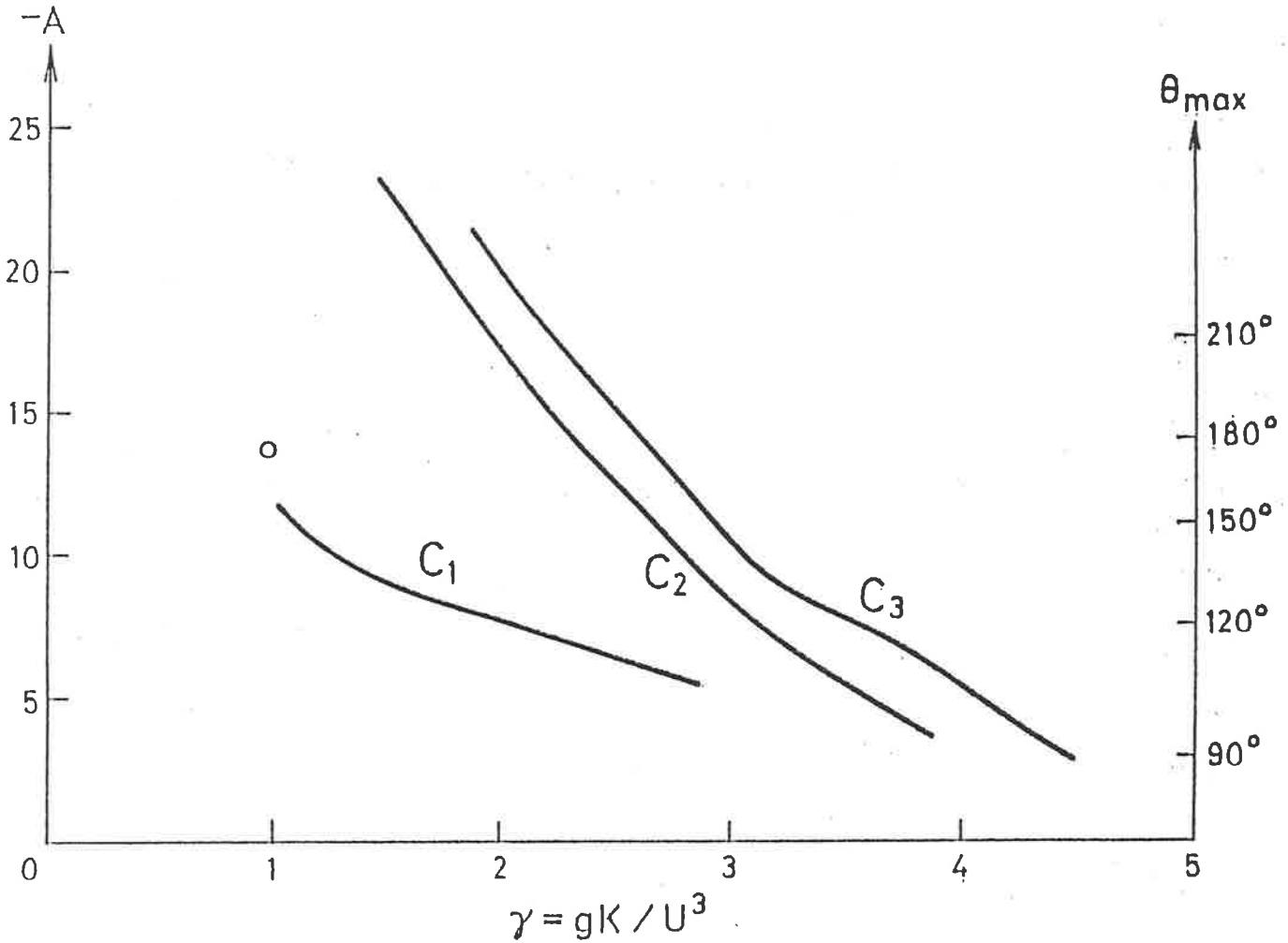

Figure 3.2.b: Variation of the body parameter A(or Θ_{max}) vs. γ at $b = .2$. The circle near the end of the C_1-curve is the result of Tuck and Vanden Broeck(1984).

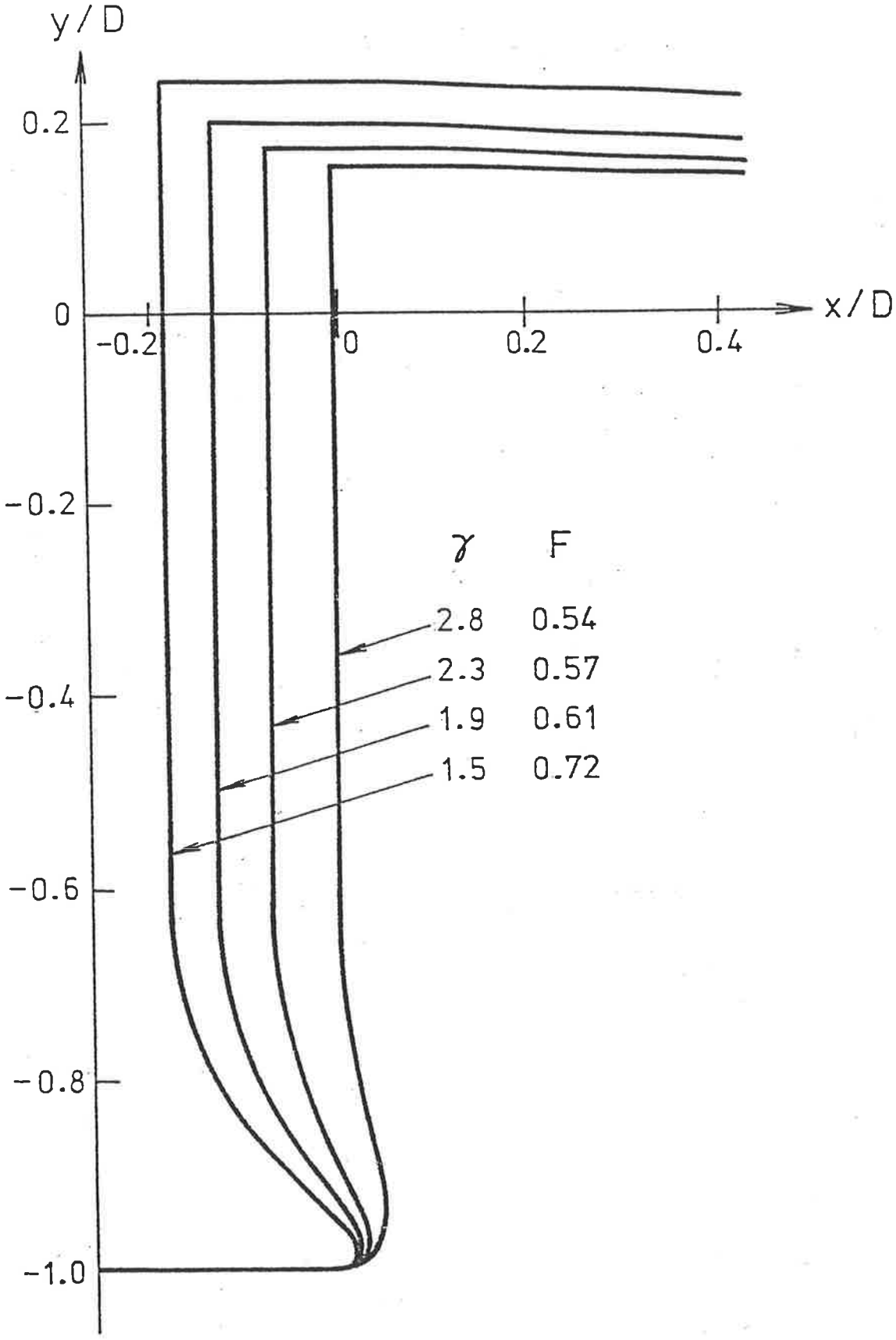

Figure 3.3: Some profiles correspond to family C_1 at $b = .3$.

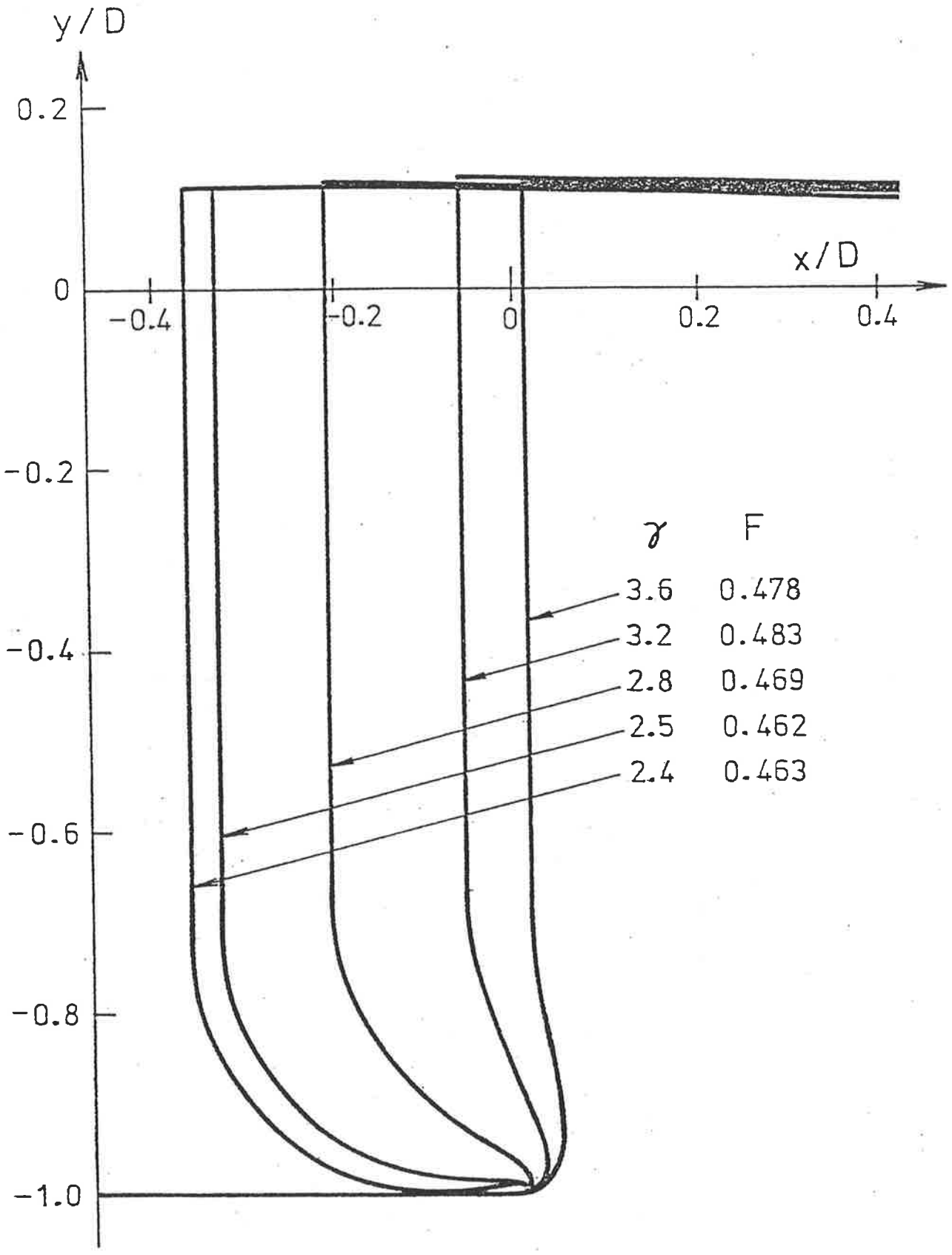

Figure 3.4: Some profiles corespond to family C_2 at $b = .3$.

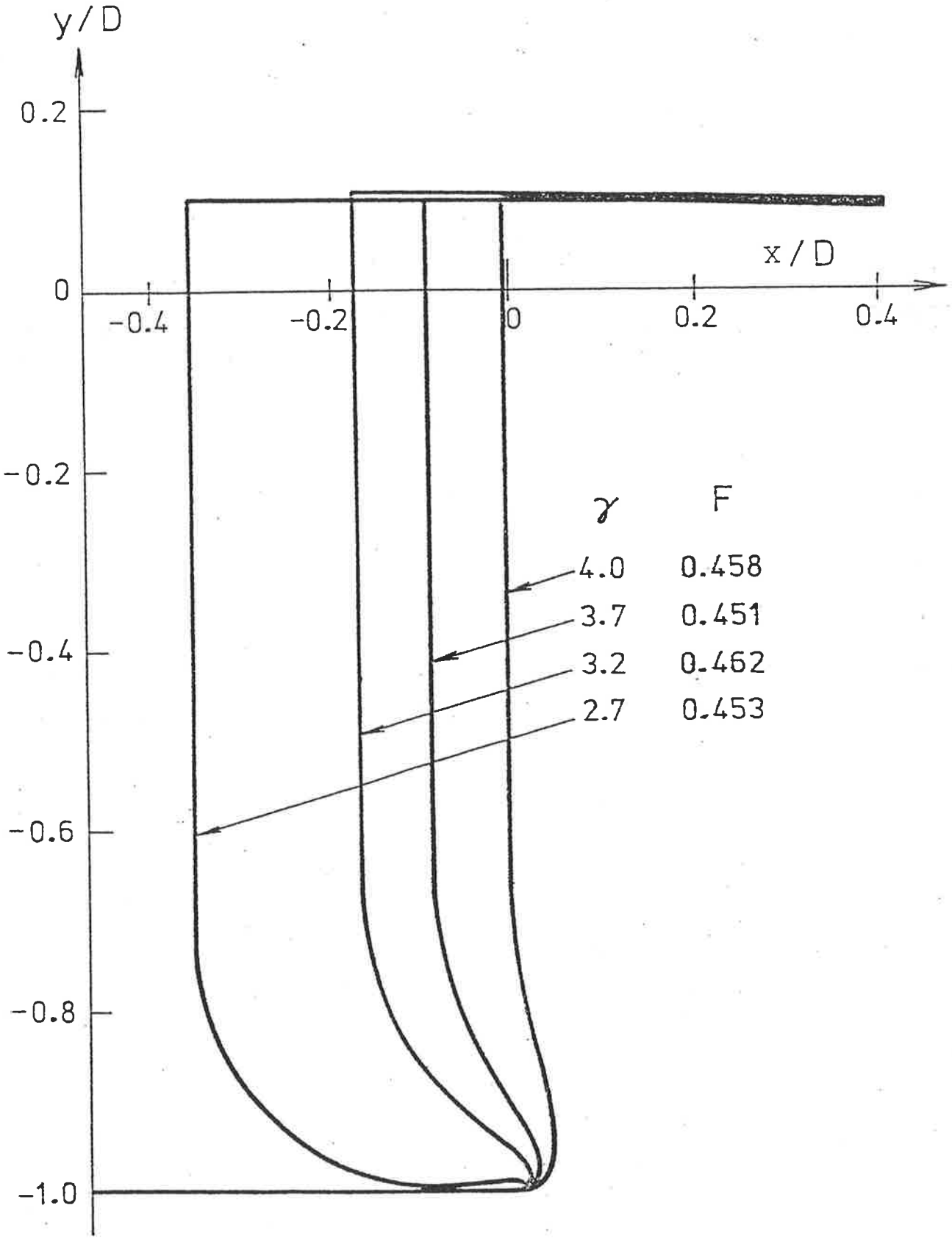

Figure 3.5: Some profiles corespond to family C_3 at $b = .3$.

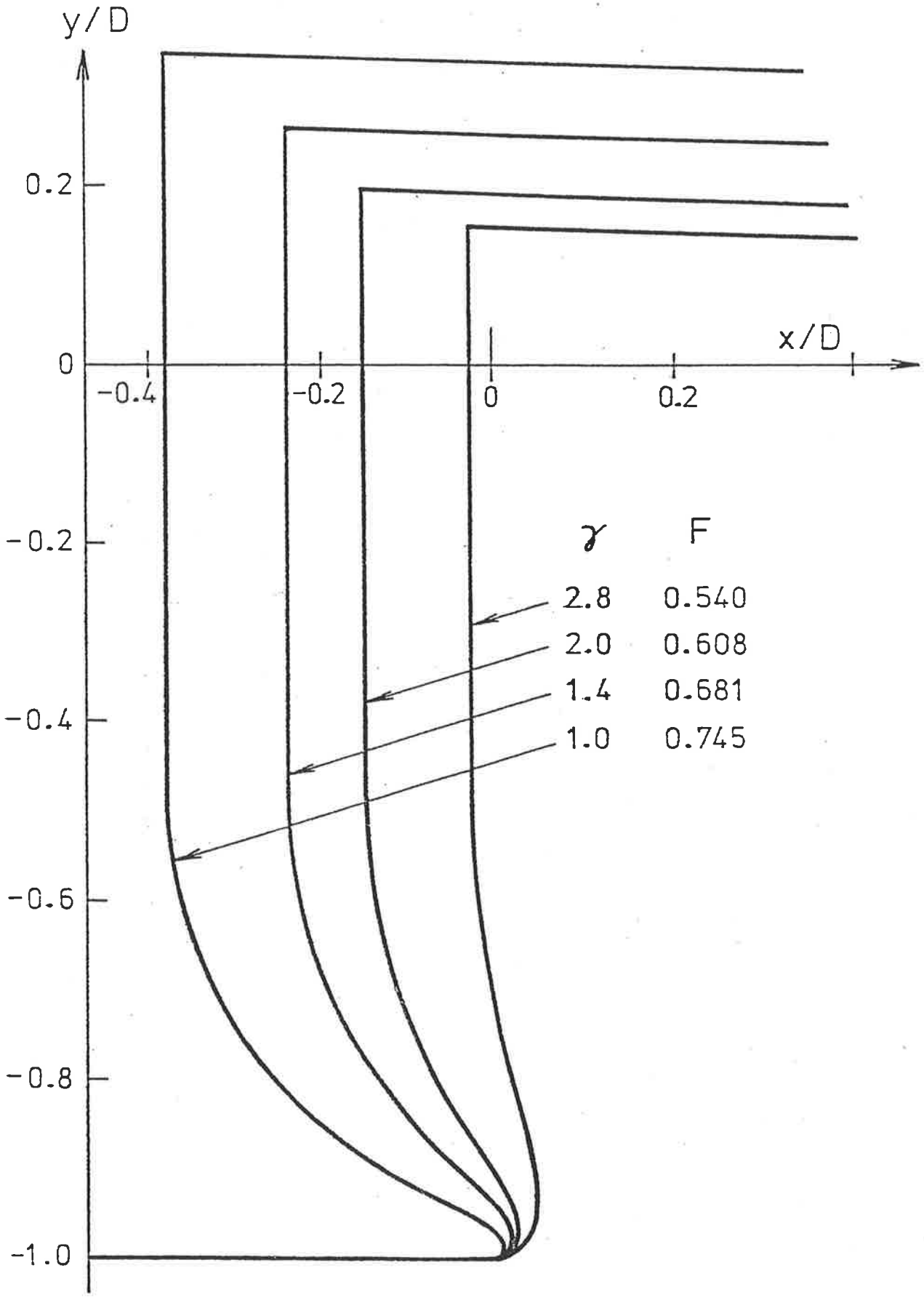

Figure 3.6: Some profiles corespond to family C_1 at $b = .2$.

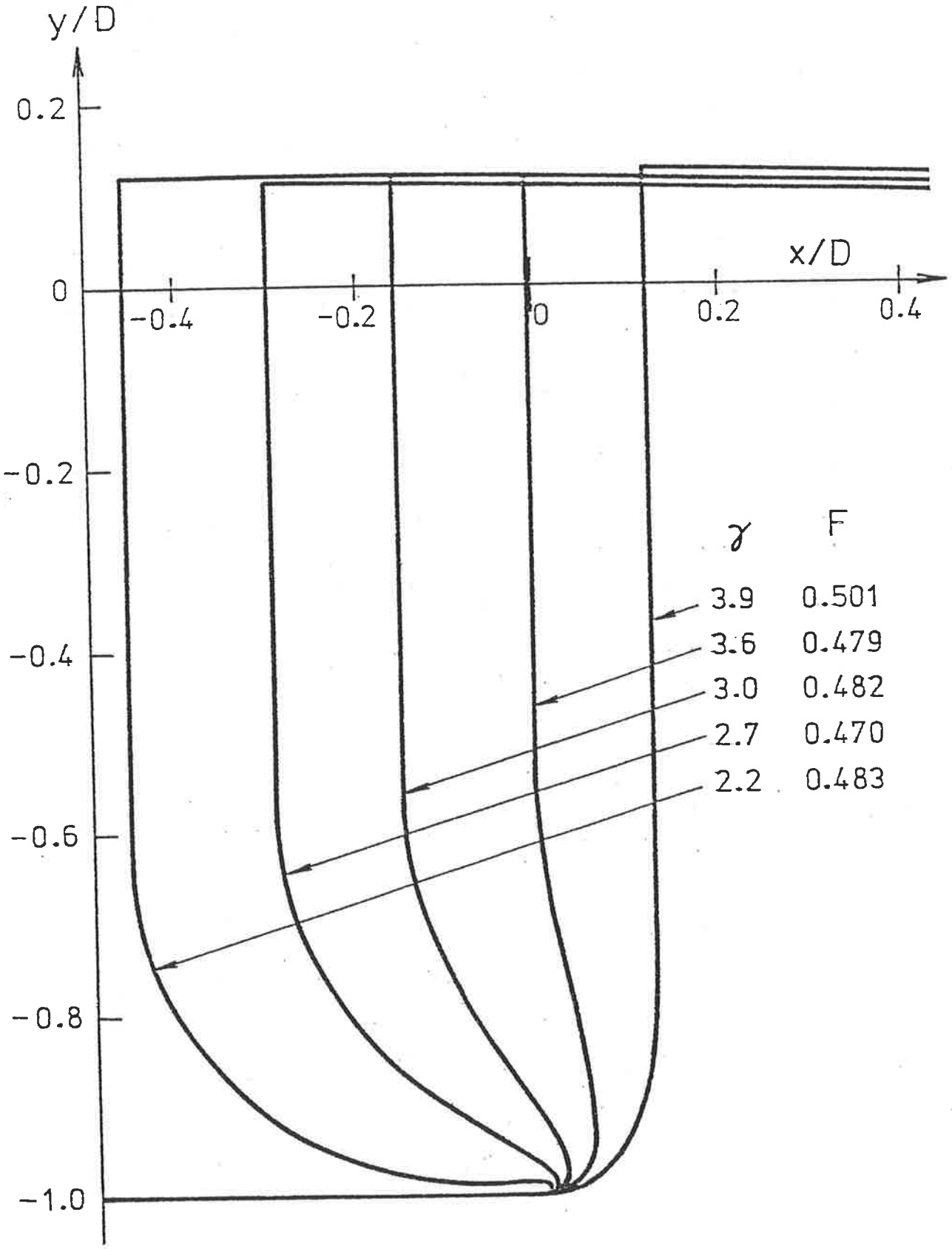

Figure 3.7: Some profiles corespond to family C_2 at $b = .2$.

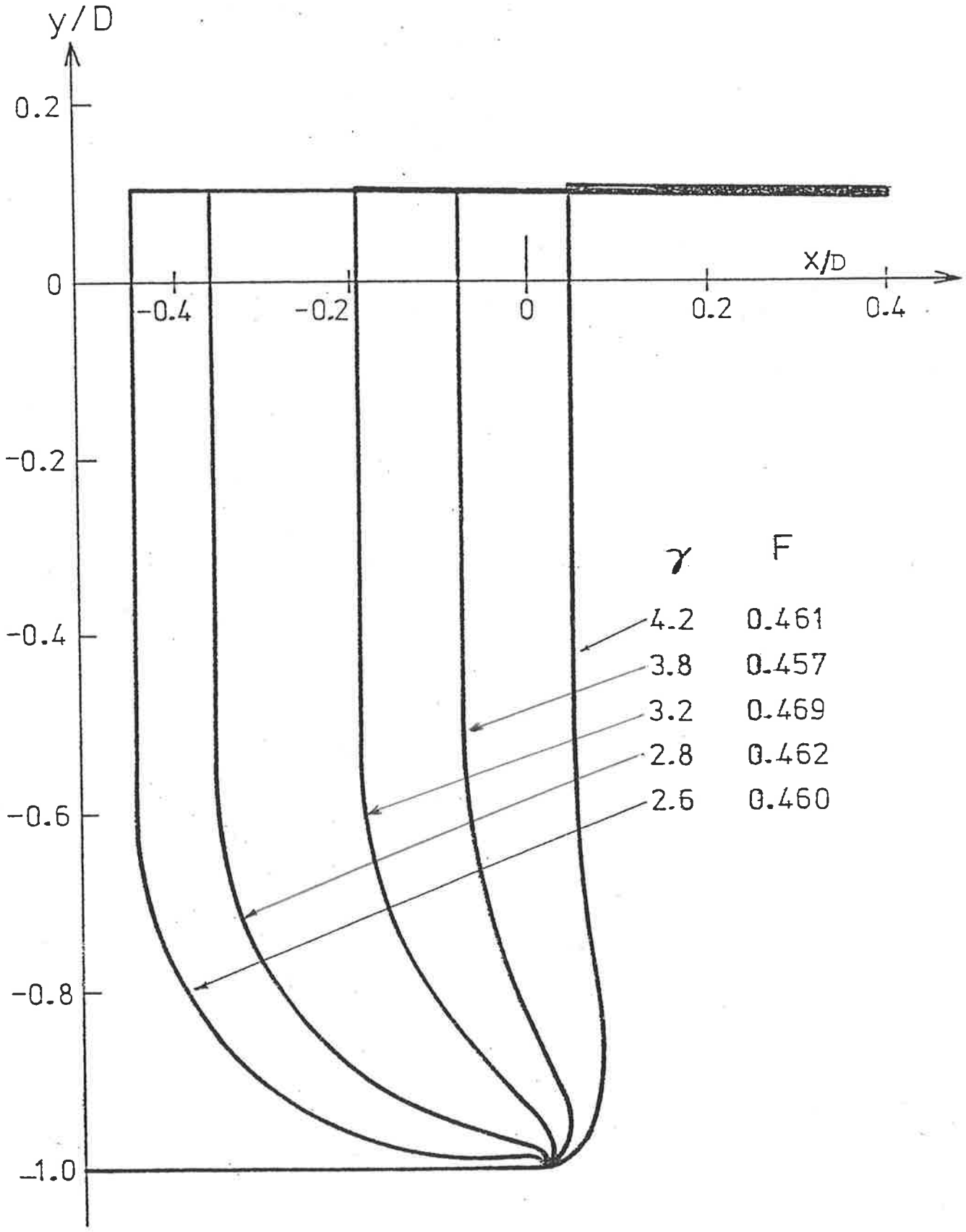

Figure 3.8: Some profiles corespond to family C_3 at $b = .2$.

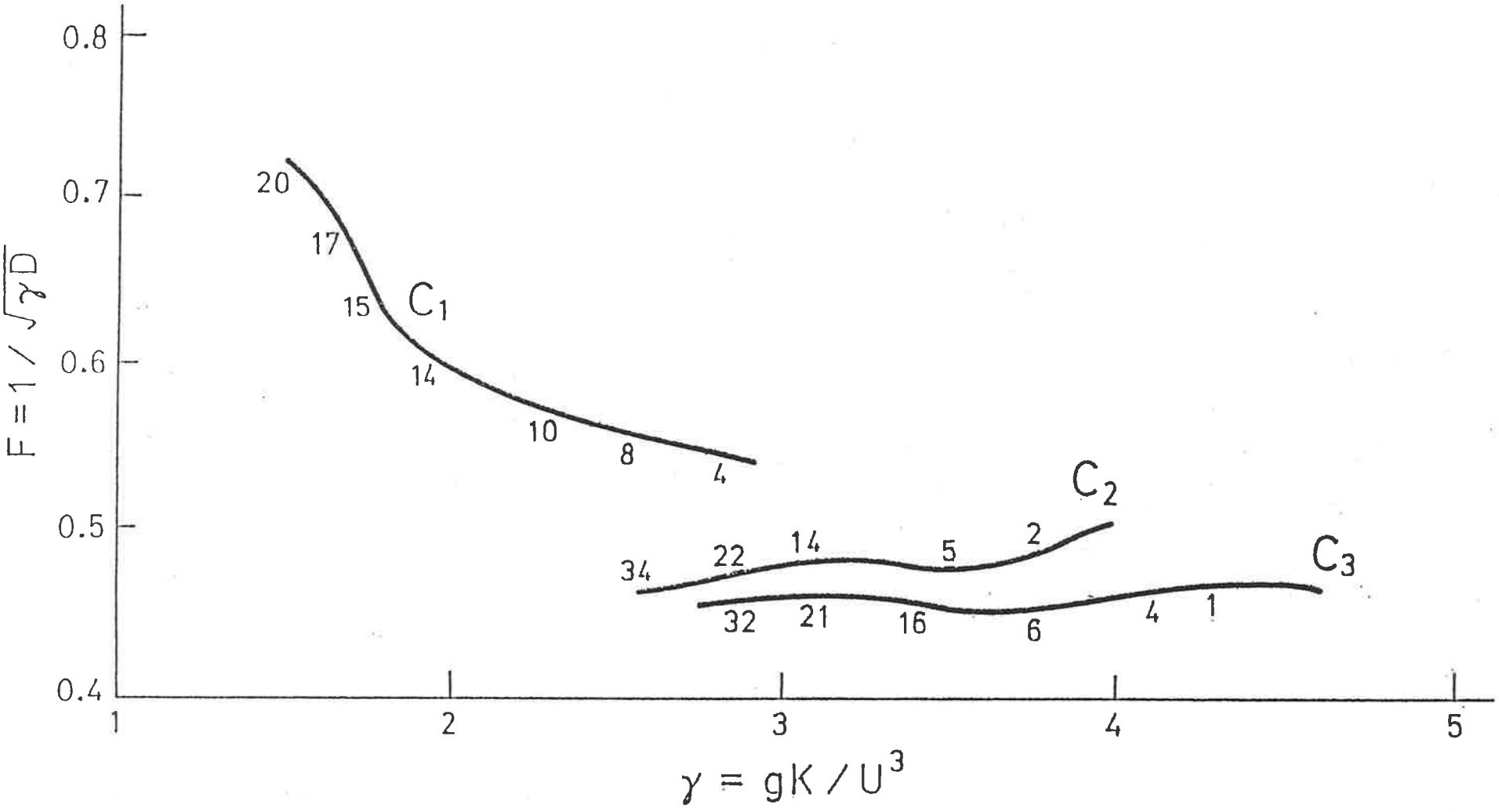

Figure 3.9.a: Variation of the Froude number vs. γ ($b = .3$). The figures marked on the curves show the protrusion ratio (B/D).

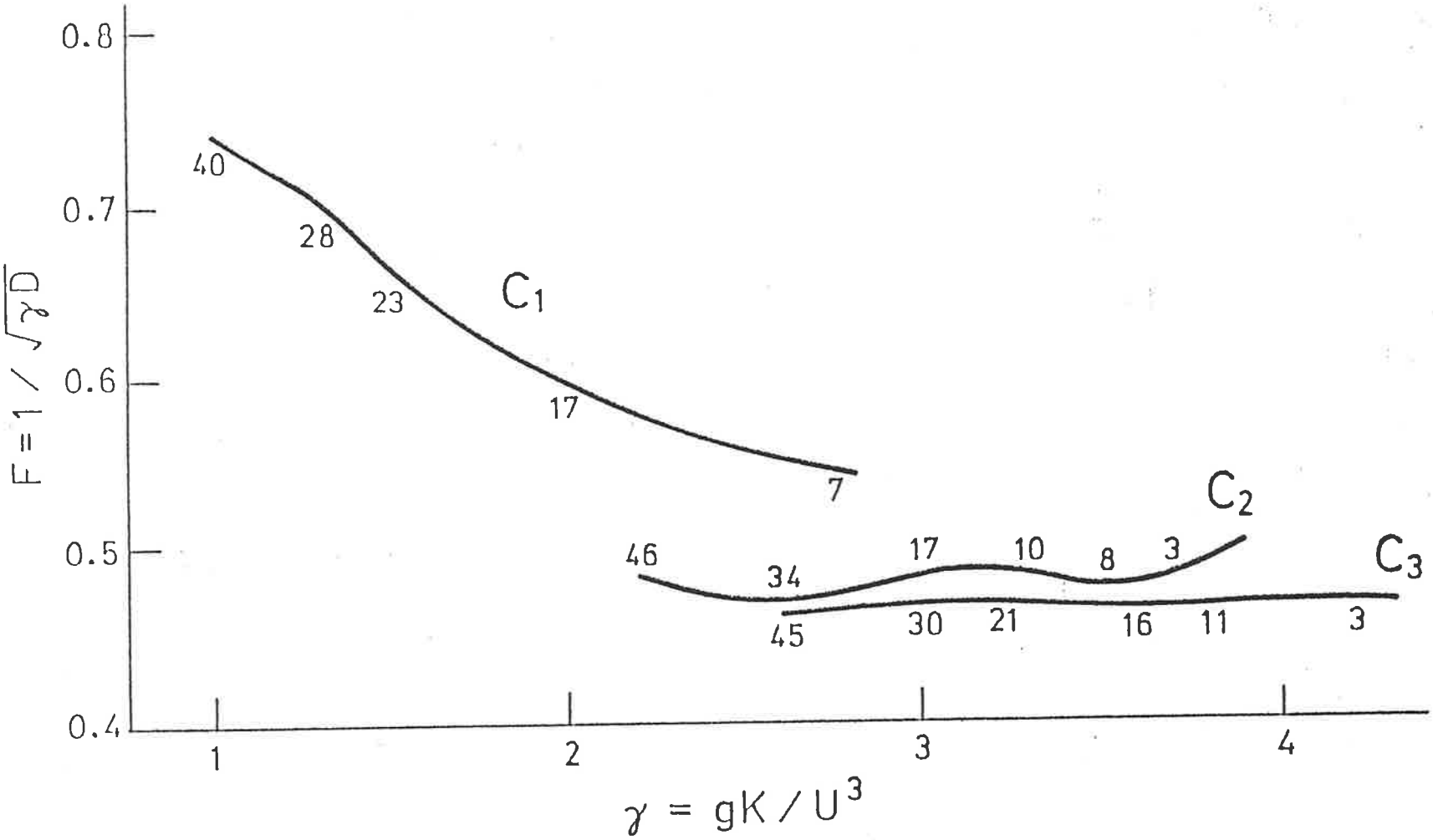

Figure 3.9.b: Variation of the Froude number vs. γ ($b = .2$).

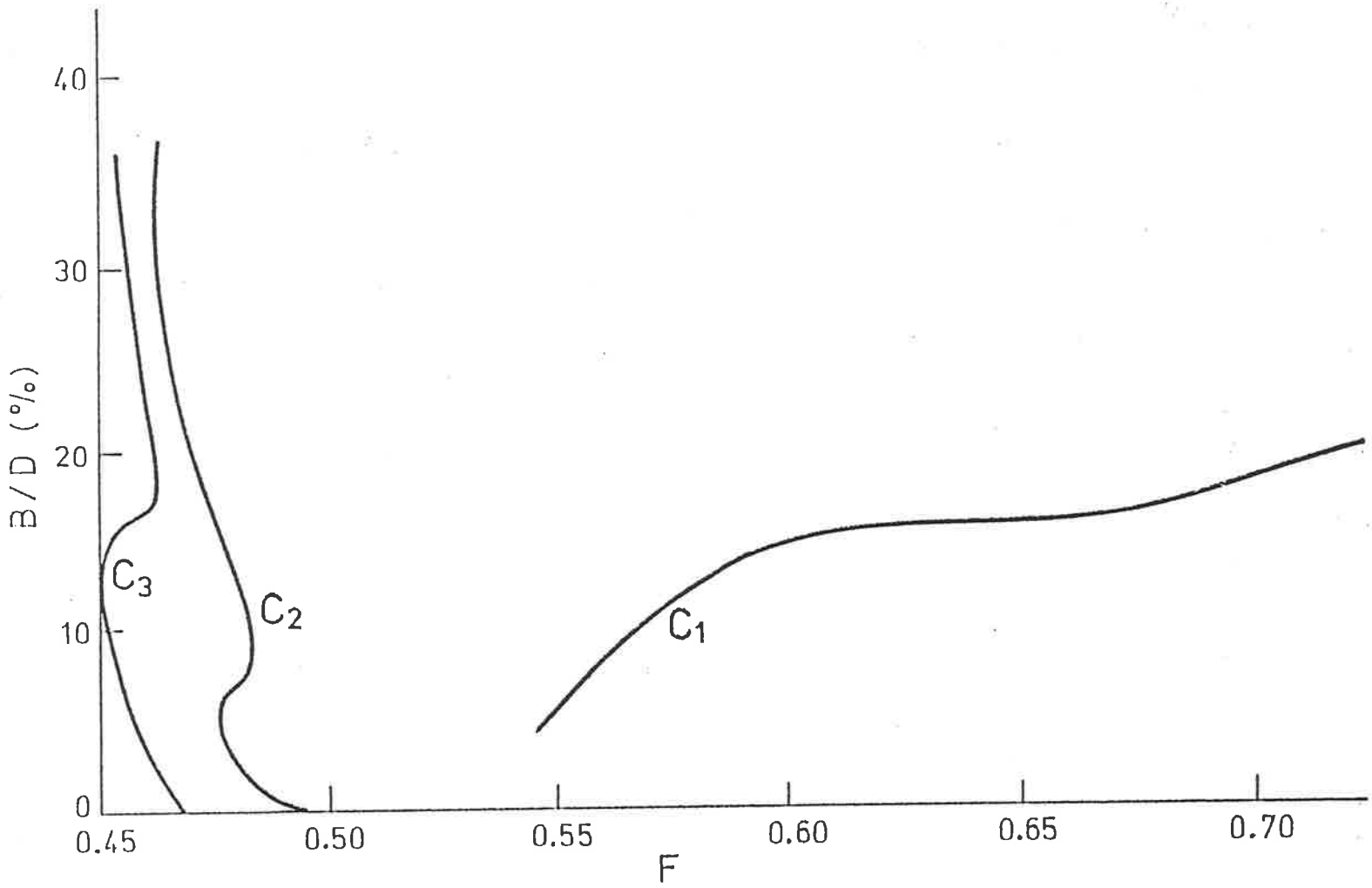

Figure 3.10.a: Protrusion of the bulb (B/D) vs. Froude number at $b = .3$.

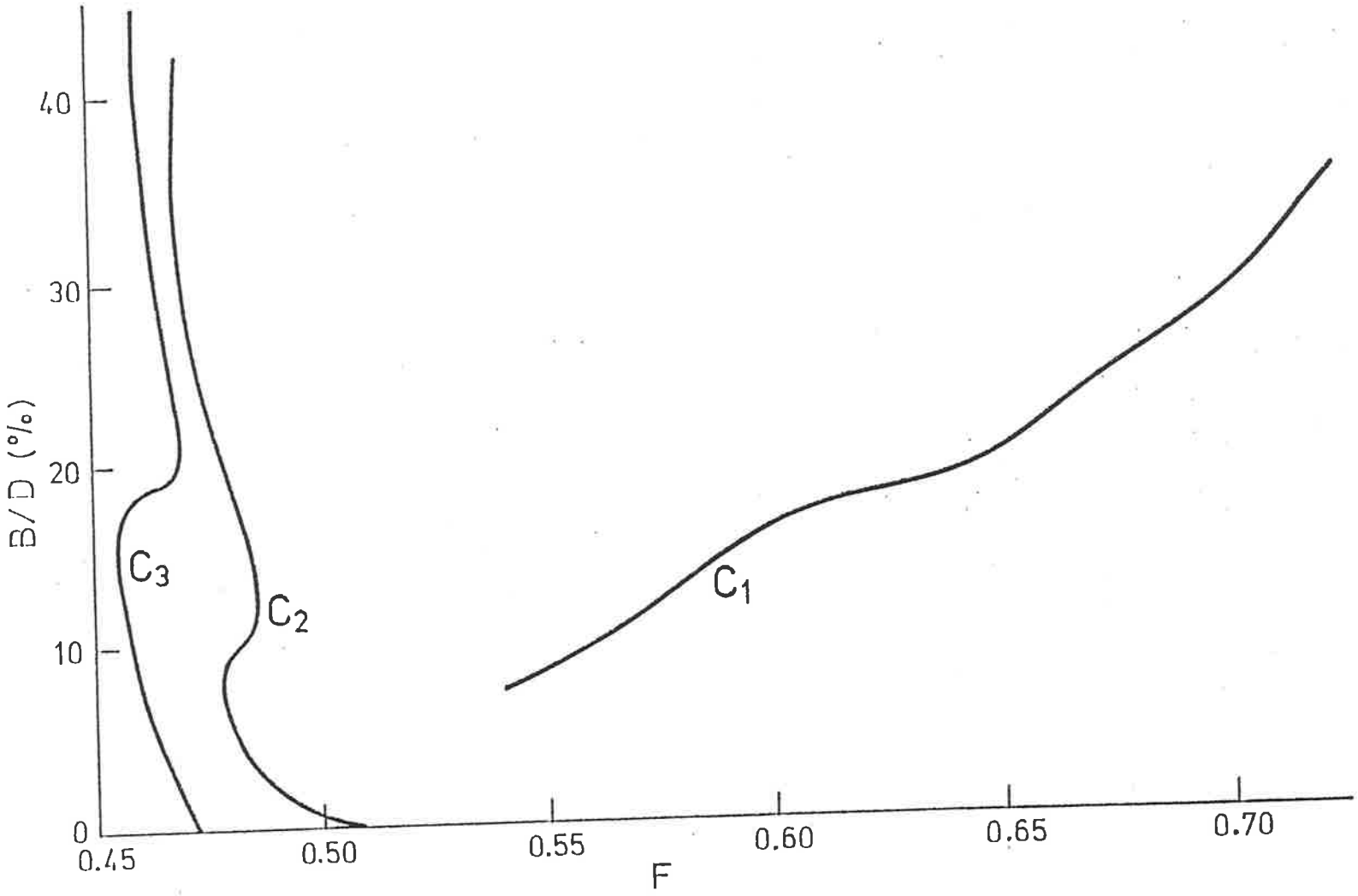

Figure 3.10.b: Protrusion of the bulb (B/D) vs. Froude number at $b = .2$.

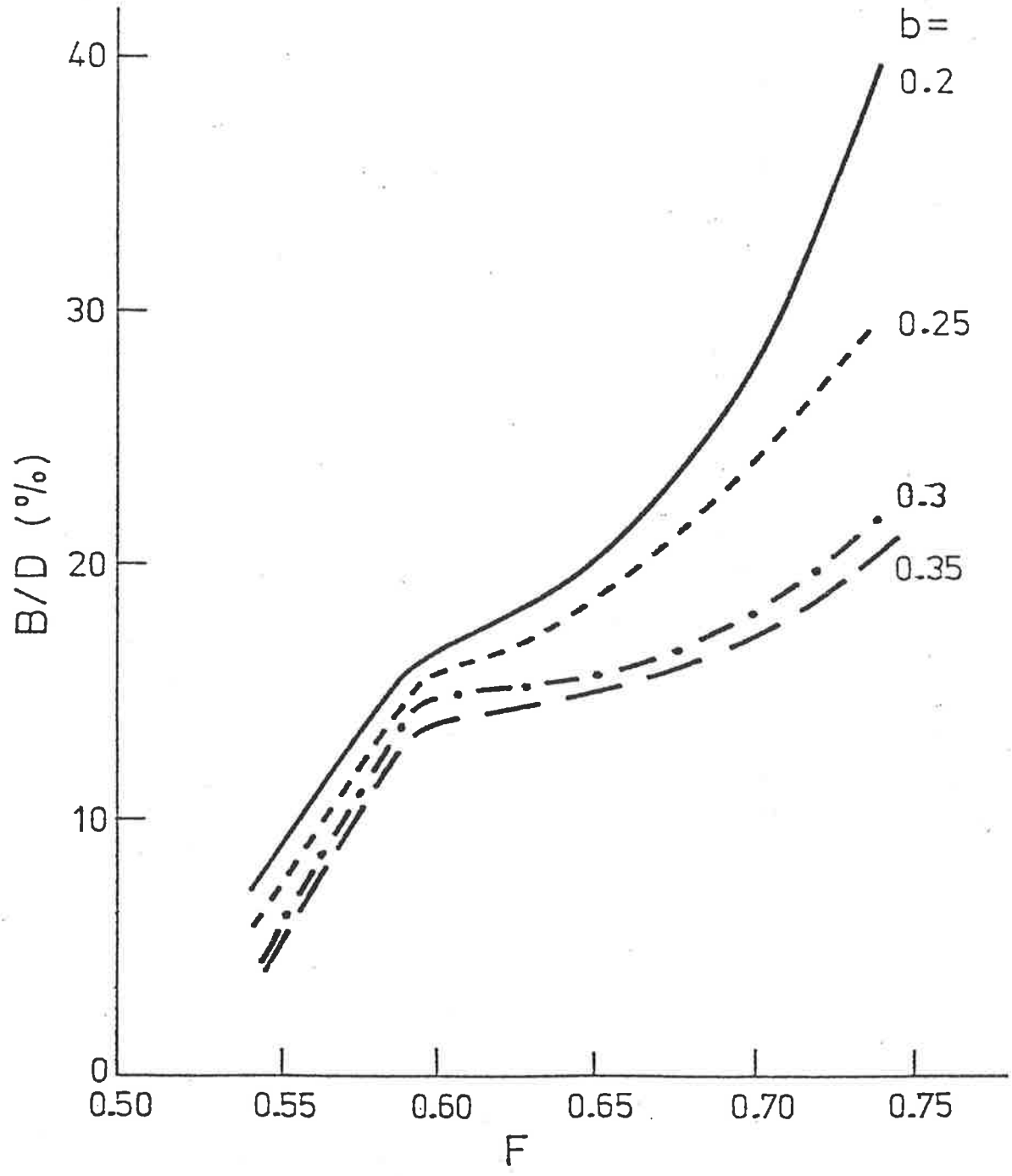

Figure 3.11.a: Variation of the bulb size (B/D) vs. Froude number for several values of b(C_1 solutions only).

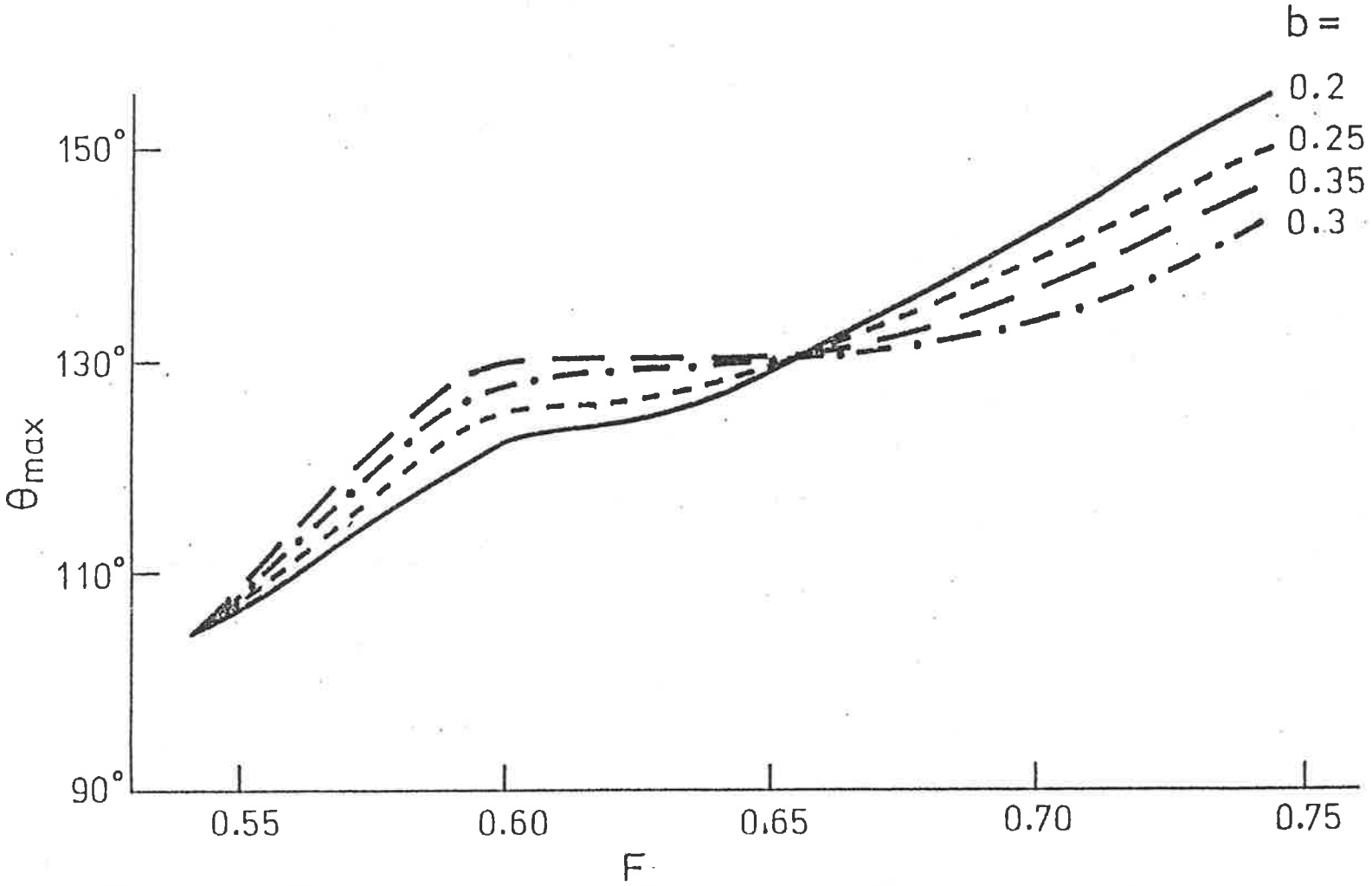

Figure 3.11.b: Maximum slope Θ_{max} vs. F for several values of $b(C_1$ solutions only).

REFERENCES

[1] Schmidt, G.H.,"Linearized stern flow of a two-dimensional shallow-draft ship", *J. Ship Res.* 25(1981), 236-242.

[2] Tuck, E.O.,and Vanden-Broeck, J.-M., "Splashless bow flows in two dimensions?" *Proc. 15th Symp. Naval Hydro.* Hamburg, Sept.1984.

[3] Vanden-Broeck, J.-M., and Tuck, E.O.,"Computation of near-bow or stern flows, using series expansion in the Froude number", *Proc. 2nd Int. Conf. Num. Ship Hydro.,* Berkeley(1977).

[4] Vanden-Broeck, J.-M., Schwartz, L.W., and Tuck, E.O., "Divergent low-Froude number series expansion of nonlinear free-surface flow problems", *Proc. Roy. Soc. London.* Ser. A 361(1978),207-224.

[5] Vanden-Broeck, J.-M., and Tuck, E.O., "Wave-less free-surface pressure distributions", *J. Ship Res.*, Vol.29,No.3,Sept 1985, pp.151-158.

[6] Madurasinghe, M.A.D., and Tuck, E.O., "Ship bows with continuous and splashless flow attachment", *J. Austral. Math. Soc.* Ser. B, Vol 27, Part 4, pp.442-452(1986).

[7] Thomas C. Gillmer, *Modern ship design*, United States Naval Institute, Maryland, 1970.

[8] Baba, E., " A new component of viscous resistance", *J. Soc. Nav. Arch.* Japan 125,23 (1969).

[9] Baba, E., "Wave breaking resistance of Ships", *In Proc. Int. Seminar on Wave resistance*, Tokyo, pp.75-92 (1976).

[10] Baba, E., " Blunt Bow Forms and Wave Breaking", *STAR-ALPHA Symposium, SNAME* Washington, D.C. (1975).

[11] Dagan, G., and Tulin, M.P., " Two dimensional free-surface gravity flow past blunt bodies." *Journal of Fluid Mech.*, Vol. 51, No.3, pp529-543 (1972).

[12] Inui, T., Kajitani, H., Miyata, H., Tsuruoka, M., Suzuki, A., and Ushio, T. "Non-Linear Properties of Wave Making Resistance of Wide-Beam Ships." *Jour. of the Soc. of Naval Arch. of Japan*, Vol. 146, pp. 18-26(1979).

[13] Inui, T., "Asymptotic Expansions Applied to Problems in Ship Waves and Wave Resistance", *Proc. 5th National Congress for Applied Mechanics*, Japan, 1956.

[14] Inui, T., "Wave-Making Resistance of Ships", *Trans. SNAME*,Vol.70,1962.

[15] Inui, T., "Study on Wave-Making Resistance of Ships", *60th Aniversary Series, Society of Naval Architects of Japan*, Vol.2,1957.

[16] Inui, T., "Japanese Developments on the Theory of Wave-Making and Wave Resistance", *Proc. 7th International Conference on Ship Hydrodynamics.* ITTC, Oslo, Aug. 19-20,1954.

[17] Inui., T., "From Bulbous Bow to Free-Surface Shock Wave - Trends of 20 Years Research on Ship Waves at the Tokyo University Tank", *Journal of Ship Res.*, Vol.25, No3, pp147-180, 1981.

[18] Oertel, R.P., "The steady motion of a flat ship including an investigation of local flow near the bow" Ph.D Thesis, Applied Mathematics Department, University of Adelaide, South Australia, July 1975.

[19] Birkhoff, G., and Zarantonello, E.H., *Jets, wakes and cavities* Academic Press, New York,(1957).

[20] Gilbarg, D.,"A Generalization of the Schwartz Christoffel transformation". *Proc. Nat. Acad. Sci. U.S.A.* 35(1949),609-612.

[21] Gilbarg, D.,"Jets and cavities", *Handbuch der Physik* Vol.9, 311-445 (Springer-Verlag, Berlin, 1960).

[22] Milne-Thomsom, L.M., *Theoretical hydrodynamics* (Macmillan, London, 1968).

[23] Wu, T.Y.,"Cavity and wake flows", *Ann. Rev. Fluid Mech.* 4(1972),243-284.

[24] Madurasinghe, M.A.D., " Splashless Ship Bows With Stagnant Flow Attachment", *Journal of Ship Research* (Submitted) Dec. 1986.

APPENDIX

(Corrections)

p.6 Line 6: 'passs' should be 'pass'.

p.7 Sentence before equation (1.3) should begin 'In the absence of gravity ....'.

p.10 Line after equation (1.13): 'thckness' should be 'thickness'.

p.13 Line 2: 'extremly' should be 'exteremely'.

p.14 Figure legend 'boubdary' should be 'boundary'.

p.28 Second paragraph 'attchment' should be 'attachment'.

p.34 Line 3: 'framework' is one word, not two.

p.50 Line 9: The reference to Vanden-Broeck and Tuck should be [2], not[6] .

p.72 Reference [22] 'Thomsom' should be 'Thomson'.